Tmbim5 loss causes muscle atrophy in zebrafish without exacerbating mcu or slc8b1 knockout phenotypes

Iga Wasilewska[1,4#], Dobrochna Adamek-Urbańska[2], Sofiia Baranykova[3], Łukasz Majewski[3], and Axel Methner[4#]

Running title: TMBIM5 Fish

[1]Mossakowski Medical Research Institute, Polish Academy of Sciences, 5 Pawinskiego Str., 02-106 Warsaw, Poland

[2]Department of Ichthyology and Biotechnology in Aquaculture, Institute of Animal Sciences, Warsaw University of Life Sciences, Ciszewskiego 8 St., 02-786 Warsaw, Poland

[3]International Institute of Molecular and Cell Biology in Warsaw, 4 Ks. Trojdena Str., 02-109 Warsaw, Poland

[4]University Medical Center of the Johannes Gutenberg-University Mainz, Institute for Molecular Medicine, Langenbeckstr. 1, D-55131 Mainz, Germany.

[#]Correspondence should be addressed to: Axel Methner MD, University Medical Center of the Johannes Gutenberg-University Mainz, Institute for Molecular Medicine, Langenbeckstr. 1, D-55131 Mainz, Germany, Tel.: +49-6131-17-2695, Email: axel.methner@gmail.com or to Iga Wasilewska, Mossakowski Medical Research Institute, Polish Academy of Sciences, 5 Pawinskiego Str., 02-106 Warsaw, Poland, Email: iwasilewska@imdik.pan.pl

The final character count: 76260

I agree with publication:

Name	**Email**	**Orcid**	**Signature**
Iga Wasilewska	iwasilewska@imdik.pan.pl	0000-0001-6402-881X	
Dobrochna Adamek-Urbańska	dobrochna_adamek@sggw.edu.pl	0000-0002-3840-935X	
Sofiia Baranykova	sbaranykova@iimcb.gov.pl	0009-0001-5400-8986	
Łukasz Majewski	lmajewski@iimcb.gov.pl	0000-0001-6797-2101	
Axel Methner	<axel.methner@gmail.com>	0000-0002-8774-0057	

Abstract

Mitochondria generate ATP by creating a proton gradient across the inner membrane. This gradient also drives calcium uptake by the mitochondrial calcium uniporter (MCU) complex, while NCLX, encoded by *SLC8B1,* facilitates efflux. Mcu deficiency in various species does not result in obvious phenotypes, suggesting the existence of additional calcium transport systems. We here generated zebrafish lacking Tmbim5, a potential bidirectional mitochondrial calcium transporter, and Slc8b1, the probable NCLX ortholog. *tmbim5* knockout fish exhibited impaired growth, muscle atrophy, increased brain cell death, and reduced mitochondrial membrane potential, but no significant changes in steady-state mitochondrial calcium levels. Slc8b1-deficient fish had increased larval mortality but were otherwise normal. Double knockouts of *tmbim5*/*mcu* and *tmbim5*/*slc8b1* were viable with normal Mendelian distribution, indicating robust compensatory mechanisms maintain calcium homeostasis. *tmbim5* knockout rescued the increased mortality in Slc8b1-deficient fish, and the NCLX inhibitor CGP-37157 lost its effect on behavior in Tmbim5-deficient but not Slc8b1-deficient zebrafish, implying shared, possibly antagonistic pathways. These findings suggest alternative pathways for mitochondrial calcium transport compensate for the loss of these proteins, enabling zebrafish survival.

Key words (5, alphabetical): *In vivo* Ca^{2+} measurements / Ion fluxes / Mcu / Nclx / Tmbim5 /

Introduction

Mitochondria generate ATP by harnessing a proton and electron gradient generated by the electron transport system. The negative mitochondrial membrane potential across the inner mitochondrial membrane also acts as the driving force for the uptake of the universal cellular messenger calcium (Ca^{2+}). Increased mitochondrial Ca^{2+} levels enhance oxidative phosphorylation, which leads to increased ATP production. Mitochondria also serve as cellular Ca^{2+} sinks, making mitochondrial Ca^{2+} uptake important for cellular Ca^{2+} signaling in general. Therefore mitochondrial Ca^{2+} homeostasis is a finely tuned process that involves the coordinated action of Ca^{2+} transporters, regulatory proteins, and interactions with the endoplasmic reticulum (ER).

The mechanisms governing mitochondrial Ca^{2+} transport are not fully understood. The mitochondrial Ca^{2+} channel mediating inward Ca^{2+} flux is the mitochondrial Ca^{2+} uniporter (MCU) (Baughman *et al*, 2011; De Stefani *et al*, 2011) which is part of a large protein complex which contains several MCU-interacting and regulatory proteins like MICU1 (mitochondrial uptake 1) (Mallilankaraman *et al*, 2012b), MICU2 (Patron *et al*, 2014), EMRE (essential MCU regulator) (Vais *et al*, 2016) and MCUR1 (mitochondrial Ca^{2+} uniporter regulator 1) (Vais *et al*, 2015; Mallilankaraman *et al*, 2012a). *Mcu* knockout (KO) in mice leads to mild phenotypes in a CD1 background (Pan *et al*, 2013) but embryonic lethality in C57Bl/6 (Murphy *et al*, 2014). In zebrafish, *mcu* knockdown did not alter survival or activity in zebrafish larvae (Soman *et al*, 2017). Also *mcu* KO had no effect on viability, fertility, morphology or swimming behavior in zebrafish although it abolished mitochondrial Ca^{2+} uptake similar to the well-characterized MCU inhibiting compound ruthenium red (RuR) (Soman *et al*, 2019a; Tomar *et al*, 2019; Langenbacher *et al*, 2020). However, *in vivo* studies in zebrafish photoreceptors suggest alternative Ca^{2+} entry pathways that can compensate for Mcu loss (Bisbach *et al*, 2020). One disputed candidate is Leucine Zipper And EF-Hand Containing Transmembrane Protein 1 (LETM1), identified by a genome-wide screen as a RuR-sensitive mitochondrial Ca^{2+}/H^{+}-antiporter (Jiang *et al*, 2009). Originally, LETM1 was described as part of the mitochondrial K^{+}/H^{+} exchanger (Nowikovsky *et al*, 2004). Ca^{2+} efflux is primarily mediated by the Na^{+}/Ca^{2+} exchanger NCLX (Palty *et al*, 2010), whose knockout causes embryonic lethality in mice (Luongo *et al*, 2017). Recent evidence suggests that also Transmembrane Protein 65 (TMEM65) is involved in Na^{+}-dependent Ca^{2+} efflux from mitochondria (Vetralla *et al*, 2023; Zhang *et al*, 2023) and may act as a positive regulator of NCLX (Garbincius *et al*, 2023). Another mitochondrial Ca^{2+} extrusion system is the mitochondrial permeability transition pore (mPTP), a non-selective high-conductance pore of debated identity (Bernardi *et al*, 2023; Altschuld *et al*, 1992). High mitochondrial Ca^{2+} concentrations lead to opening of the mPTP which, when sustained, causes mitochondrial swelling, breakdown of mitochondrial membrane potential, and eventually cell death (reviewed in (Orrenius *et al*, 2015)).

Recently, a novel candidate for mitochondrial Ca^{2+} transport emerged, the transmembrane BAX inhibitor motif containing protein 5 (TMBIM5) initially linked to the regulation of mitochondrial morphology, as loss of TMBIM5 in cells resulted in mitochondrial fragmentation and a disrupted cristae structure (Oka *et al*, 2008; Seitaj *et al*, 2020; Zhang *et al*, 2022; Austin *et al*, 2022). Loss of TMBIM5 was also observed to increase the sensitivity of cells to apoptosis (Oka *et al*, 2008; Seitaj *et al*, 2020; Patron *et al*, 2022). In *vivo*, mice genetically engineered with a specific alteration (D326R) that presumably disrupts the channel pore of the TMBIM5 protein (Bultynck *et al*, 2014) and leads to degradation of the protein (Zhang *et al*, 2022) exhibit several significant physiological and structural changes. These mice show a higher mortality during embryonic development or shortly after birth and develop a skeletal myopathy characterized by reduced muscle strength. These observations

were closely linked to several mitochondrial abnormalities most dramatically obvious in mitochondria obtained from skeletal muscle. This included a disrupted cristae structure, premature mPTP opening, decreased ability of mitochondria to take up Ca^{2+}, and swollen mitochondria (Zhang *et al*, 2022).

Two studies demonstrated that TMBIM5, when reconstituted in liposomes, can act as a Ca^{2+} transporter in the presence of a pH gradient (Patron *et al*, 2022; Austin *et al*, 2022). Inhibiting NCLX-mediated mitochondrial Ca^{2+} efflux by CGP-37157 (CGP) (Austin *et al*, 2022) or *NCLX* knockdown (Patron *et al*, 2022) resulted in a diminished mitochondrial Ca^{2+} retention capacity in *TMBIM5* KO in human embryonic kidney (HEK) cells and reduced RuR-induced mitochondrial Ca^{2+} efflux (Austin *et al*, 2022). *TMBIM5* KO cells also accumulated more matrix Ca^{2+} upon ER Ca^{2+} release mediated by inhibition of the sarco/endoplasmic ATPase (SERCA) with thapsigargin (Patron *et al*, 2022) or stimulation of inositol trisphosphate receptor-mediated Ca^{2+} release with ATP or carbachol (Austin *et al*, 2022). Concurrent knockout of *MCU* rescued elevated apoptosis induced by staurosporine in *TMBIM5*$^{-/-}$ cells (Patron *et al*, 2022), suggesting that TMBIM5 can mediate Ca^{2+} extrusion from mitochondria and that its function at least partially overlaps with NLCX. Zhang et al., in contrast, found that TMBIM5 overexpression in HEK cells enhanced mitochondrial Ca^{2+} uptake following ER Ca^{2+} release (Zhang *et al*, 2022), suggesting that TMBIM5 may operate bidirectionally under certain conditions. This study also demonstrated that under steady-state conditions, loss of TMBIM5 results in increased potassium and reduced proton levels in the mitochondrial matrix suggesting a broader role in mitochondrial ion exchange (Zhang *et al*, 2022) in line with a potential interaction of TMBIM5 with LETM1 (Austin *et al*, 2022). The physiological significance of these mechanisms *in vivo*, especially the crosstalk of TMBIM5 with MCU and NCLX, is unclear.

Due to their translucency, zebrafish are an ideal tool to study mitochondrial Ca^{2+} dynamics *in vivo* (Kettunen, 2020; Mandal *et al*, 2018). In the present study, we generated *tmbim5* and *slc8b1* KO fish by CRISPR/Cas9-mediated gene editing (Gasanov *et al*, 2021) and observed that loss of Tmbim5 results in a muscle phenotype associated with delayed hatching, smaller size, and increased cell death in the brain while loss of Slc8b1 resulted in increased larvae mortality. In living larvae, Tmbim5 depletion did not affect mitochondrial Ca^{2+} levels. CGP reduced swimming velocity and distance in wildtype but not in *tmbim5* KO fish. To investigate potential interactions with known Ca^{2+} transport systems, we generated *tmbim5*/*mcu* and *tmbim5*/*slc8b1* double knockouts. Both lines were viable without major phenotypes. Concurrent Tmbim5 deletion actually reduced the mortality seen in *slc8b1* KO larvae and did not exacerbate it. The mild phenotypes of double knockouts indicate either strong compensatory mechanisms or that additional Ca^{2+} transport pathways maintain mitochondrial Ca^{2+} homeostasis in the absence of these proteins.

Results

Tmbim5-deficient larvae are smaller and exhibit a reduced hatching efficiency

The zebrafish genome contains only one *TMBIM5* orthologue which is expressed as early as six hours post fertilization (hpf) and plateaus after 24 hours (Fig. 1A). To study the effect of Tmbim5 deficiency, we generated mutant fish by introducing a deletion in exon 4 using CRISPR/Cas9 genome editing (Gasanov *et al*, 2021). This resulted in a profound decrease in *tmbim5* mRNA (Fig. 1B); mutants (*tmbim5*$^{-/-}$) reached adulthood and the Mendelian distribution was unchanged (Fig. 1C). Mutant larvae took longer to hatch than wild-type (WT, *tmbim5*$^{+/+}$) controls (Fig. 1D) and this correlated with reduced tail coiling (Fig. 1E), spontaneous movements of the tail that enable the embryo to escape from its chorion (Lessman & Carver, 2014). This suggested a possible reduction in muscle strength as also

observed in mice with a channel pore mutation in TMBIM5 (Zhang *et al*, 2022). Despite that, mutant larvae displayed unchanged spontaneous locomotor activity in an open field test (Fig. EV1A) as well as after stimulating mobility in a visual-motor response test (Fig. EV1B). Tmbim5-deficient larvae were morphologically normal (Fig. 1F) but shorter, had a smaller eye diameter and thinner somites (Fig. 1G). This reduction in somite thickness was not solely attributable to the overall reduction in whole-body size, as the ratio of somite thickness to whole-body length was also decreased in *tmbim5*$^{-/-}$ larvae (Fig. 1G). Together these results suggest a role for Tmbim5 in body size and muscle strength.

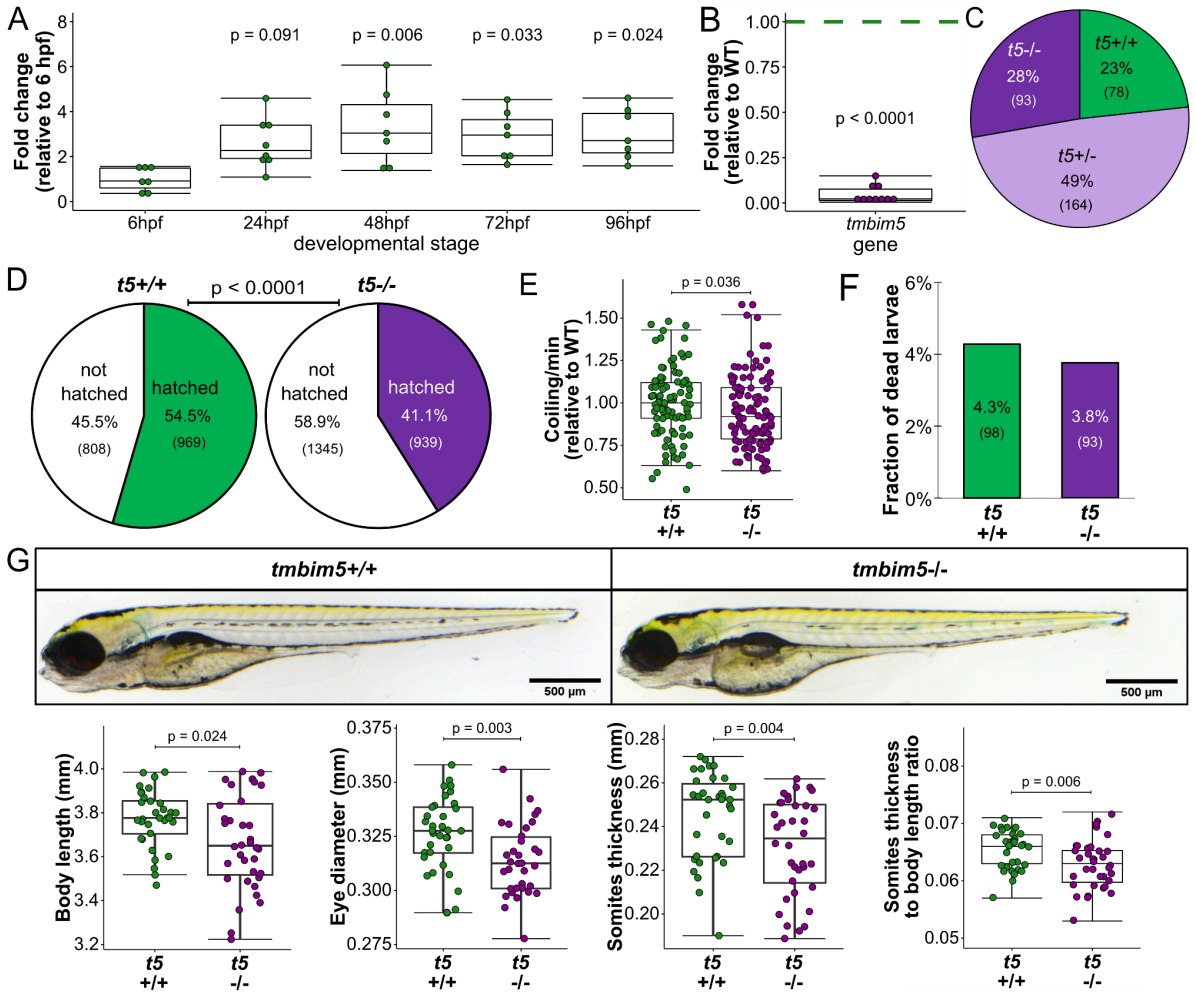

Figure 1. Tmbim5-deficient larvae are smaller and exhibit a reduced hatching efficiency

A) *tmbim5* mRNA levels at different developmental stages estimated using quantitative PCR (qPCR), *18S* was used as a reference gene, expression normalized to 6 hpf. Data plotted as box and whisker plots with the box representing the 25-75th percentile and the whiskers indicating min to max, each dot representing an independent biological replicate, n = 7-8 (each RNA sample was isolated from 30 embryos/larvae), number of experiments = 4, one-way ANOVA followed by post-hoc Tukey HSD test, p values for comparisons with 6 hpf.

B) Decreased *tmbim5* mRNA level in 5dpf *tmbim5*$^{-/-}$ larvae quantified with qPCR and normalized to WT, *rpl13a* and *ef1a* were used as reference genes. Data plotted as box and whisker plots with the box representing the 25-75th percentile and the whiskers indicating min to max, each dot representing an independent biological replicate, n = 10 (each RNA sample was isolated from 30 larvae), number of experiments = 5, one sample *t* test.

C) Genotype distribution does not differ from expected after *tmbim5* (*t5*)$^{+/-}$ zebrafish breeding. Compared to Mendelian distribution, n is indicated in brackets, number of experiments = 4, Chi-square test.

D) Reduced hatching of *tmbim5*$^{-/-}$ larvae. n is indicated in brackets, number of experiments = 6, Chi-square test.

E) Reduced coiling activity of 1 dpf *tmbim5*$^{-/-}$ embryos, mean number of coiling movements during 1 min normalized to WT from the same experiment were plotted as box and whisker plots with the box representing the 25-75th percentile and the whiskers

indicating min to max, each dot representing an individual embryo, n = 94-104, number of experiments = 6, one-sample Wilcoxon test.

F) Mortality of *tmbim5*$^{-/-}$ larvae until 5 dpf is not affected. n is indicated in brackets, number of experiments = 7, Chi-square test.

G) Abnormal morphology of 5dpf *tmbim5*$^{-/-}$ larvae. Representative images of WT (*tmbim5*$^{+/+}$) and *tmbim5*$^{-/-}$ larvae and the results of morphometric analysis were plotted as box and whisker plots with the box representing the 25-75th percentile and the whiskers indicating min to max, each dot representing an individual larvae, n = 34-36, number of experiments = 3, Mann–Whitney test (body length and somites thickness) or *t* test.

Adult Tmbim5-deficient fish weigh less, show signs of muscle atrophy and decreased glycogen levels in muscle and liver

We next studied the effects of Tmbim5 deficiency in adult zebrafish. Similar to larvae, *tmbim5*$^{-/-}$ adult fish had a normal morphology, a tendency to be smaller and a significant reduction in weight compared to WT fish (Fig. 2A).

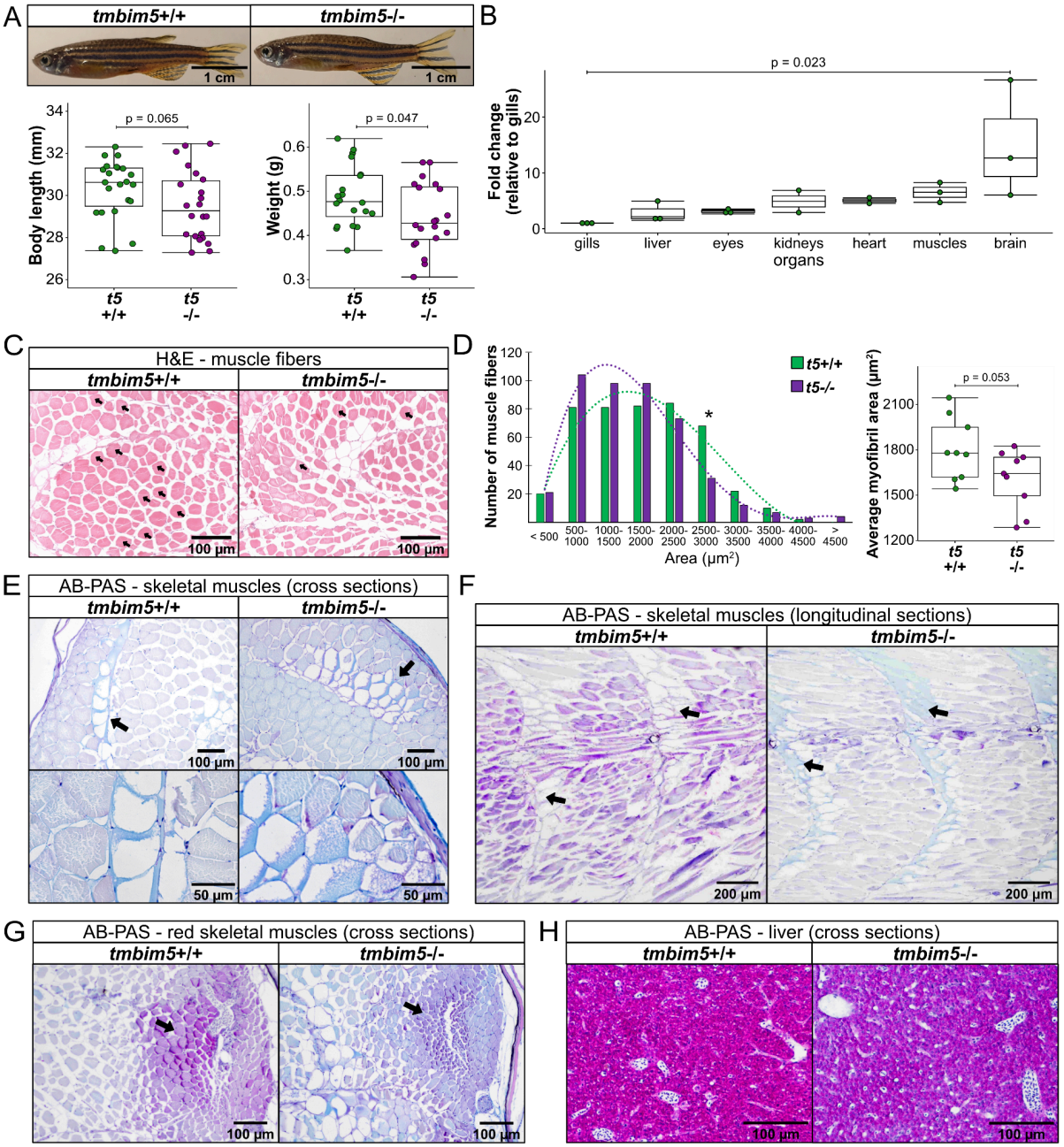

Figure 2. Adult Tmbim5-deficient fish weigh less, show signs of muscle atrophy and decreased glycogen levels in muscle and liver

A) Smaller size of *tmbim5*$^{-/-}$ adult fish. Representative images of WT and *tmbim5*$^{-/-}$ 8 month-old zebrafish and the results of morphometric analysis were plotted as box and whisker plots with the box representing the 25-75th percentile and the whiskers indicating min to max, each dot representing an individual fish, n = 19-23, number of experiments = 3 (weight) or 4 (body length), Mann–Whitney test (body length) or *t* test (weight).

B) *tmbim5* mRNA levels in organs of adult zebrafish estimated using qPCR: *rpl13a* was used as a reference gene, expression normalized to gills (organ with the lowest *tmbim5* expression level). Data plotted as box and whisker plots with the box representing the 25-75th percentile and the whiskers indicating min to max, each dot representing an independent biological replicate, n = 2-3, (each RNA sample was isolated from 2 fish), number of experiments = 3, Kruskal-Wallis test followed by Dunn's test.

C) Smaller cross-sectional area of muscle fibers of *tmbim5*$^{-/-}$ adult fish. Representative images of WT and *tmbim5*$^{-/-}$ 8 month-old H&E stained zebrafish skeletal muscles. Arrows indicate fibers of 2500-3000 μm^2, which number is significantly reduced in the mutants.

D) Histogram of the morphometric analysis of muscle fibers in WT and *tmbim5*$^{-/-}$ fish shows the distribution of cross-sectional area of muscle fibers is different in mutants than in WT and shifted towards smaller fibers in the mutants, Chi-square test (p = 0.0009). Differences in the number of fibers of particular sizes are marked with an asterisk, Mann–Whitney test or *t* test with BH correction for the multiply comparisons. On the right, box and whisker plots with the box representing the 25-75th percentile and the whiskers indicating min to max presenting trend for the reduction in the average myofibril area in the mutants, each dot representing an average for one slice (50 fibers analyzed per slice), n = 9, number of fish = 3, *t* test.

E-F) Enhanced Alcian blue (AB) staining of intermuscular spaces of *tmbim5*$^{-/-}$ fish. Representative images of E) cross sections, below magnification of the area of AB-stained intermuscular spaces marked with arrow, and F) longitudinal section of WT and *tmbim5*$^{-/-}$ fish stained with AB-PAS (Periodic Acid-Schiff).

G) Lower intensity of PAS staining indicates reduced glycogen level in the muscles of *tmbim5*$^{-/-}$ fish. Representative images of cross-sections of WT and *tmbim5*$^{-/-}$ fish stained with AB-PAS.

H) Glycogen level is reduced also in the liver of *tmbim5*$^{-/-}$ fish, as indicated by decreased PAS staining intensity. Representative images of cross sections of WT and *tmbim5*$^{-/-}$ fish stained with AB-PAS.

Locomotor activity of adult fish was unchanged (Fig. EV1C). The larger size of adult fish allowed us to perform a histopathological analysis of brain and muscle, the tissues with the highest mRNA expression levels of *tmbim5* (Fig. 2B). A histopathological examination of brain tissue revealed no obvious differences (Fig. EV2A-D). However, a morphometric analysis of muscle fibers demonstrated a shift towards smaller fibers in the mutants (Fig. 2C) and a decline in the fibers with a cross-sectional area of 2500-3000 μm^2 (Fig. 2D). The average cross-sectional area of myofibrils was also reduced in *tmbim5*$^{-/-}$ fish (Fig. 2D). Staining muscle tissue with Alcian blue revealed an increased staining of the intermuscular space (Fig. 2E-F). Alcian blue stains acid mucopolysaccharides, which can accumulate abnormally in certain muscle disorders. This staining is also regularly used to identify rimmed vacuoles or myxoid changes which can occur in certain myopathies and degenerative conditions (Tuckett & Morriss-Kay, 1988). Such enhanced Alcian blue staining was previously observed after knockout of the mitochondrial core transcription factor *Tfam* (*mitochondrial transcription factor A*) in vascular smooth muscle cells where this correlated with reduced oxygen consumption rates and increased lactate production (Oller *et al*, 2021). Masson's staining (Fig. EV2E-F) was unchanged, excluding the possibility that Alcian blue stained collagen fibers. This staining could reveal fibrosis that may occur as a result of myofiber degeneration (Van De Vlekkert *et al*, 2020). Furthermore, Alcian blue-Periodic Acid-Schiff (AB-PAS) staining revealed decreased glycogen levels in the muscles of adult *tmbim5*$^{-/-}$ fish (Fig. 2F-G). This was also obvious in the liver of mutant fish (Fig. 2H). Together these results imply that Tmbim5-deficient fish have signs of metabolic impairment and muscle atrophy in line with the reduced muscle strength observed in larvae. The reduced weight of adult fish aligns with the reduced size observed in larvae.

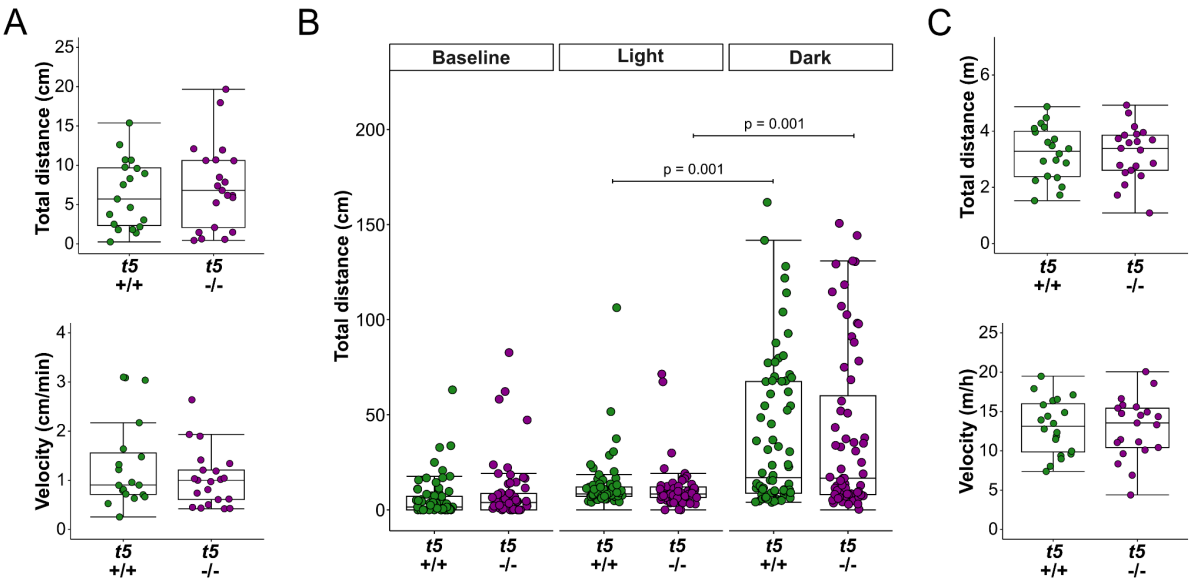

Figure EV1. Normal behavior of *tmbim5*$^{-/-}$ zebrafish.

A) Locomotor activity of 5dpf larvae in an open field test is not affected by *tmbim5* KO, total distance and mean velocity were plotted as box and whisker plots with the box representing the 25-75th percentile and the whiskers indicating min to max, each dot representing an individual larvae, n = 19-21, number of experiments = 3, *t* test (total distance) or Mann–Whitney test (velocity).

B) Normal visual-motor response of 5dpf *tmbim5*$^{-/-}$ larvae, total distance cover during each phase of the experiment was plotted as box and whisker plots with the box representing the 25-75th percentile and the whiskers indicating min to max, each dot representing an individual larvae, n = 64-72, number of experiments = 3, Kruskal-Wallis test followed by Dunn's test.

C) Locomotor activity of adult (8 month-old) fish in an novel tank test is not affected by *tmbim5* KO, total distance and mean velocity were plotted as box and whisker plots with the box representing the 25-75th percentile and the whiskers indicating min to max, each dot representing an individual fish, n = 20-21, number of experiments = 3, Mann–Whitney test.

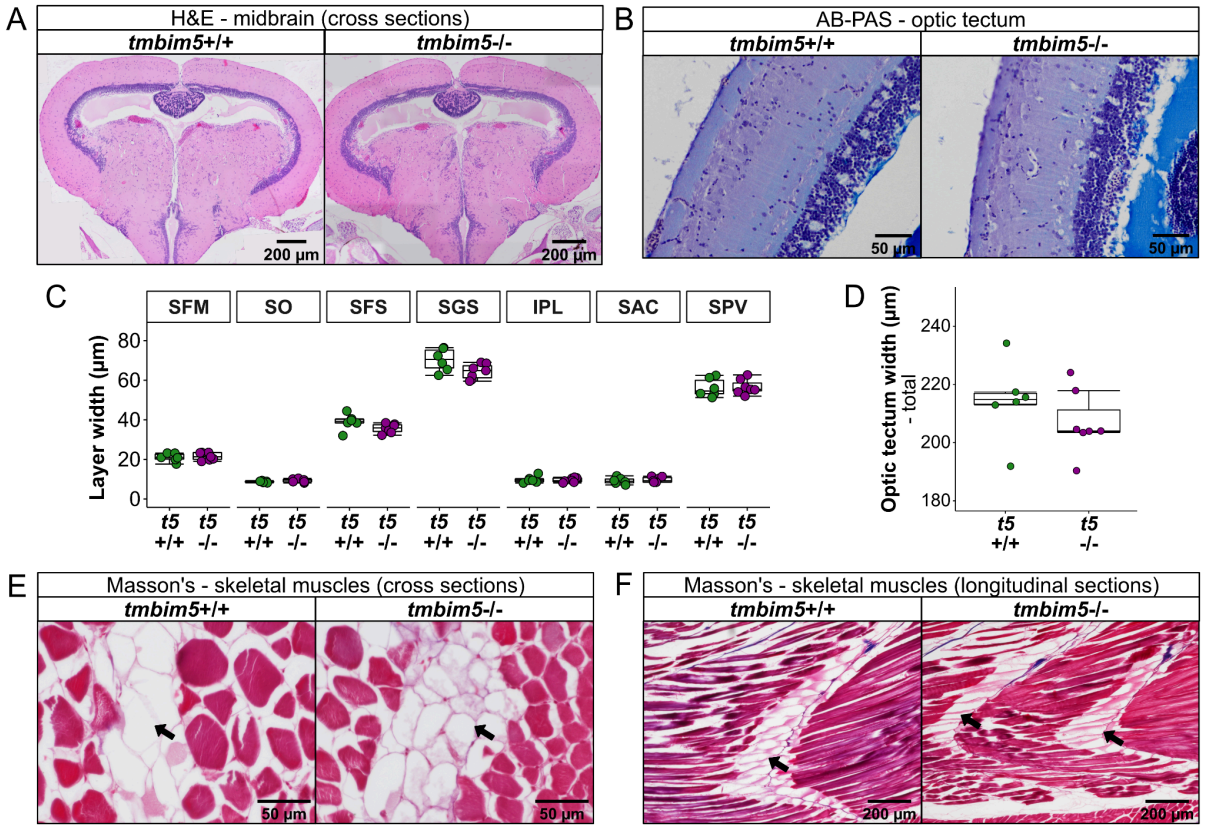

Figure EV2. No signs of fibrosis and normal histology of brain of adult *tmbim5*$^{-/-}$ fish

A-D) Normal histology of *tmbim5*$^{-/-}$ fish brain. A) Representative images of cross sections of WT and *tmbim5*$^{-/-}$ midbrain stained with H&E. B) Representative images of cross sections of WT and *tmbim5*$^{-/-}$ optic tectum stained with AB-PAS with C) quantifications of width of optic tectum layers and D) comparison of total width of optic tectum between WT and *tmbim5*$^{-/-}$ fish, that did not show any significant differences. Data presented as box and whisker plots with the box representing the 25-75th percentile and the whiskers indicating min to max, each dot representing one fish (5-7 slices analyzed for each fish, 5 measurements per slice), n = 6-7, *t* test with BH correction for the multiply comparisons. SFM - Stratum Fibrosum Superficiale, SO - Stratum Opticum, SFS - Stratum Fibrosum Superficiale, SGS - Stratum Fibrosum Griseum, IPL - Internal Plexiform Layer, SAC - Stratum Album Centrale, SPV - Stratum Periventriculare.

E-F) Masson's staining of skeletal muscles did not reveal any changes in *tmbim5*$^{-/-}$ fish. Representative images of E) cross sections and F) longitudinal sections of WT and *tmbim5*$^{-/-}$ fish stained with intermuscular spaces that showed positive AB staining marked with arrows.

Live imaging reveals unchanged mitochondrial Ca^{2+} levels in the brain of Tmbim5-deficient fish

To clarify whether changes in the mitochondrial Ca^{2+} homeostasis could explain the effects of Tmbim5 deficiency, we took advantage of the translucency of zebrafish larvae which allows the quantification of (mitochondrial) Ca^{2+} levels in the living animal using genetically-encoded Ca^{2+} sensors. We chose the hindbrain because *tmbim5* is strongly expressed there as shown by whole-mount in situ hybridization (Fig. 3A); importantly no staining was observed in *tmbim5*$^{-/-}$ larvae proving the specificity of the riboprobe. We also found increased cell death in this tissue as demonstrated by staining the brain of *tmbim5*$^{-/-}$ larvae with Acridine Orange (Fig. 3B) implying functional changes associated with Tmbim5 deficiency. We crossed *tmbim5* mutant with fish *Tg*(*CEPIA2mt*) expressing the mitochondrially targeted sensor CEPIA2mt (Suzuki *et al*, 2014) under the neuronal promoter *HuC*/*elavl3* (*ELAV like neuron-specific RNA binding protein 3*) and imaged mitochondria in the optic tectum, a dorsally located part of the hindbrain which is accessible for imaging in *tmbim5*$^{-/-}$;*Tg*(*CEPIA2mt*) and *tmbim5*$^{+/+}$;*Tg*(*CEPIA2mt*) larvae (Fig. 3A', Fig. 3C). To quantify total matrix Ca^{2+} content, we exposed immobilized living zebrafish larvae to the uncoupling agent CCCP. This induces mitochondrial depolarization and, as a consequence, a release of Ca^{2+} from mitochondria. No differences between *tmbim5*$^{+/+}$ and *tmbim5*$^{-/-}$ larvae were observed implying that Tmbim5 deficiency in larvae had no major effect on mitochondrial Ca^{2+} levels *in vivo* (Fig. 3C-D). Also inhibition of sodium-dependent Ca^{2+} extrusion using CGP before CCCP treatment did not unmask any significant changes between WT and mutant larvae (Fig. 3C-D). Experiments boosting Ca^{2+} influx with glutamate added to the bath were not successful. These results imply that *in vivo* matrix Ca^{2+} levels under conditions of physiological cytosolic Ca^{2+} levels are not affected by Tmbim5 even in the presence of CGP. To further investigate mitochondrial function in the brain of *tmbim5*$^{-/-}$ larvae, we injected tetramethylrhodamine ethyl ester (TMRE) into the yolk of zebrafish embryos at the 1-cell stage as described in (Vicente *et al*, 2019) to determine whether loss of Tmbim5 affects the mitochondrial membrane potential. TMRE is a positively charged dye known to accumulate in mitochondria due to their membrane potential. Two days after injection, we observed a TMRE signal similar to the CEPIA2mt pattern (Fig. 3C), which was significantly reduced after depolarisation with CCCP (Fig. 3E). We observed a smaller drop in TMRE signal intensity in *tmbim5*$^{-/-}$ larvae in response to depolarisation, indicating reduced dye accumulation within mitochondria and suggesting a reduced mitochondrial membrane potential in the brain of Tmbim5-deficient larvae (Fig. 3E). Together these findings suggest a potential mitochondrial dysfunction but no major differences in mitochondrial Ca^{2+} concentration in Tmbim5-deficient fish.

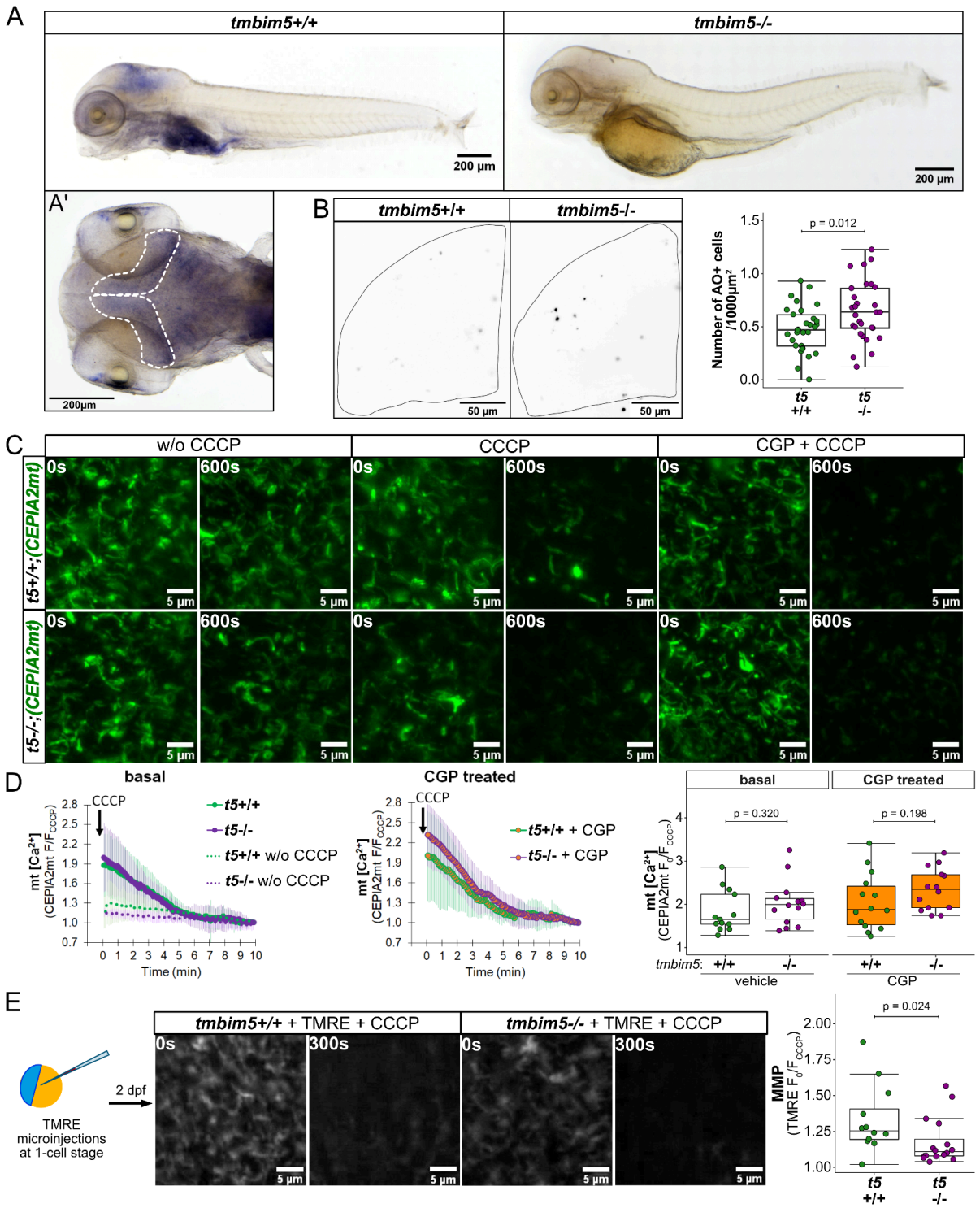

Figure 3. Live imaging reveals unchanged mitochondrial Ca^{2+} levels in the brain of Tmbim5-deficient fish

A) *tmbim5* transcript detected with whole-mount *in situ* hybridization in 4 dpf wild-type and loss of its expression in *tmbim5*$^{-/-}$ larvae. A' dorsal view with an optic tectum region outlined with a dashed line, number of experiments = 4.

B) Increased cell death in the optic tectum of *tmbim5*$^{-/-}$ larvae detected with Acridine Orange (AO) staining. Representative images of WT and *tmbim5*$^{-/-}$ larvae (black dots indicating high AO signals) and quantification results presented as box and whisker plots with the box representing the 25-75th percentile and the whiskers indicating min to max, each dot representing an individual larvae, n = 29-30, number of experiments = 3, *t* test.

C-D) No alteration in a mitochondrial Ca^{2+} response to depolarization with CCCP larvae at basal conditions and after treatment with CGP-37157 (5 µM). CCCP (10 µM) was used to depolarize mitochondria and F_0 to F_{CCCP} ratio was calculated. C) Representative images of ROI at the beginning and after 10 min of CCCP treatment. D) F_0 to F_{CCCP} mean ±SD traces and box and whisker plots with the box representing the 25-75th percentile and the whiskers indicating min to max, each dot

representing an individual larvae, n = 13-14, Two-way ANOVA followed by post hoc Dunn's test (the effect of treatment - WT), Tukey HSD test (the effect of treatment - *tmbim5*$^{-/-}$), Mann–Whitney test (the effect of genotype - WT) or *t* test (the effect of genotype - *tmbim5*$^{-/-}$).

E) Decrease in mitochondrial membrane potential in *tmbim5*$^{-/-}$ zebrafish was observed *in vivo* in the optic tectum of 2 dpf larvae. Zebrafish embryos were injected with TMRE (1 nl of 2mM) at 1-cell stage and imaged *in vivo* with LSFM at 2 dpf. CCCP (10 µM) was used to depolarize mitochondria and F_0 to F_{CCCP} ratio was calculated. On the left representative images of ROI at the beginning and after 5 min of CCCP treatment. On the right, mitochondrial membrane potential (MMP) calculated as F_0 to F_{CCCP} ratio plotted as box and whisker plots with the box representing the 25-75th percentile and the whiskers indicating min to max, each dot representing an individual larvae, n = 14-18, Mann–Whitney test.

Fish deficient in Mcu and Tmbim5 are viable

The MCU complex is the major mitochondrial Ca^{2+} uptake mechanism (Baughman *et al*, 2011; De Stefani *et al*, 2011). To clarify whether Tmbim5, as overexpression results suggested (Zhang *et al*, 2023), can modify MCU activity or act as an additional Ca^{2+} uptake mechanism besides the MCU complex, we crossed *tmbim5*$^{-/-}$ mutants with *mcu* KO fish hypothesizing that depletion of two (potentially independent) uptake mechanisms would be detrimental and/or alter mitochondrial Ca^{2+} uptake. *mcu* KO fish lack the capacity to uptake mitochondrial Ca^{2+} but have an otherwise unremarkable phenotype (Soman *et al*, 2019a). No differences in mortality were noted between *tmbim5*$^{+/+}$;*mcu*$^{-/-}$ and *tmbim5*$^{-/-}$;*mcu*$^{-/-}$ larvae (Fig. 4A) or in the distribution of adult zebrafish genotypes following a heterozygous cross (Fig. 4B). Mcu-depleted mitochondria had almost no Ca^{2+} uptake with no significant further reduction in the absence of Tmbim5 (Fig. 4C). Together these results imply that Tmbim5 does not constitute a mitochondrial Ca^{2+} uptake system independent of Mcu.

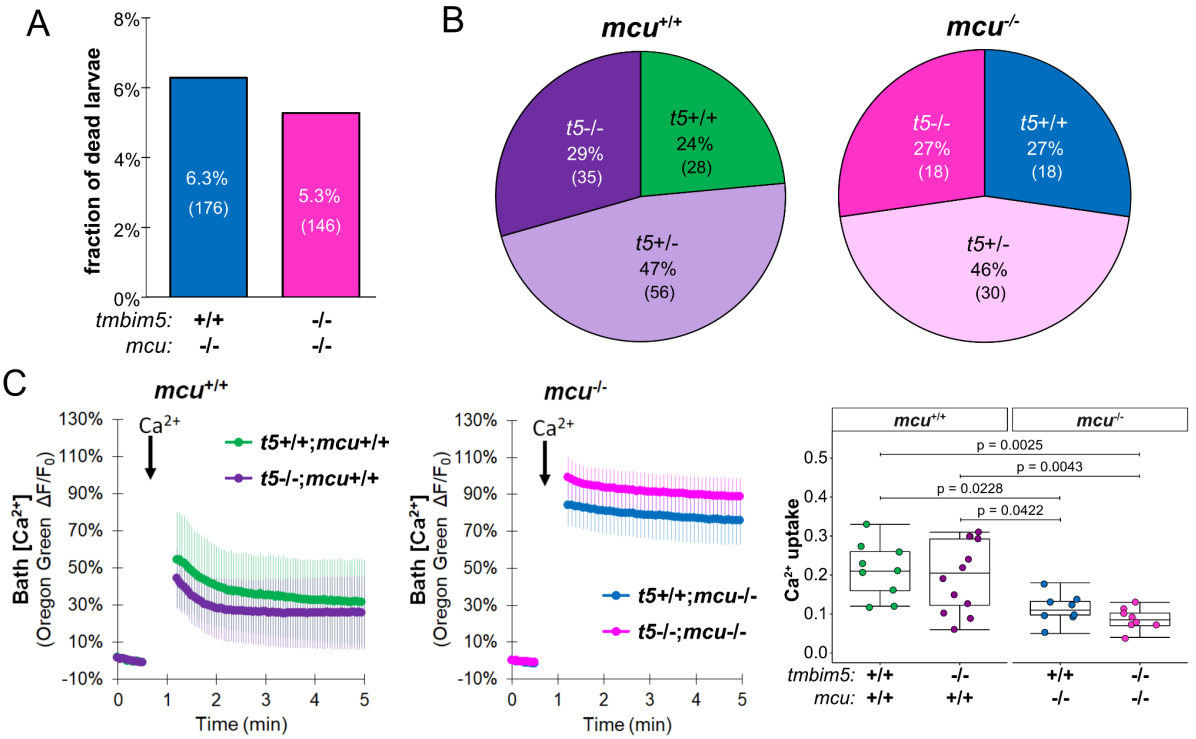

Figure 4. Fish deficient in Mcu and Tmbim5 are viable

A) Mortality of double knockout *tmbim5*$^{-/-}$;*mcu*$^{-/-}$ larvae until 5 dpf is not different from *tmbim5*$^{+/+}$;*mcu*$^{-/-}$, n is indicated in brackets, number of experiments = 4, Chi-square test.

B) Genotype distribution does not differ from expected after *tmbim5*$^{+/-}$;*mcu*$^{+/-}$ zebrafish breeding. Compared to Mendelian distribution with, n is indicated in brackets, Chi-square test.

C) No significant effect of loss of Tmbim5 on mitochondrial Ca^{2+} uptake in mitochondria isolated from *mcu*$^{-/-}$ larvae. Mitochondria were loaded with Ca^{2+} (20 µM), which revealed a significantly smaller Ca^{2+} uptake in single *mcu*$^{-/-}$ and in double *tmbim5*$^{-/-}$;*mcu*$^{-/-}$ knockouts. Fluorescence of Oregon Green 488 BAPTA-5N was normalized to the initial value (F_0). The data were presented as

mean ±SD $\Delta F/F_0$ traces. Gaps in the measurements are due to technical limitations of the equipment and procedure used, which required a pause in the fluorescence reading during reagent addition. On the right quantification of Ca^{2+} uptake. This was calculated in 2 min after $CaCl_2$ addition as a difference between maximum $\Delta F/F_0$ value after adding Ca^{2+} and $\Delta F/F_0$ reached 2 min after Ca^{2+} addition. Results presented as box and whisker plots with the box representing the 25-75th percentile and the whiskers indicating min to max, each dot representing an independent biological replicate, n = 8-12. one way ANOVA followed by a post-hoc Tukey HSD test.

No changes in the mitochondrial Ca^{2+} uptake machinery in tmbim5-deficient larvae

We next investigated the effect of tmbim5 deficiency on the expression of the mitochondrial Ca^{2+} machinery and quantified the mRNA expression levels of Mcu, Micu1-3, Efhd1, which has recently been demonstrated to interact with Mcu and suppress uniporter activity (Meng *et al*, 2023; Delgado de la Herran *et al*, 2024), and Letm1, which is also suggested to play a role in Ca^{2+} transport, along with its paralogue Letm2. Moreover, the mRNA levels of *slc8b1* (the probable NCLX ortholog) and Tmem65, which has been recently considered to be involved in Ca^{2+} efflux from mitochondria (Zhang *et al*, 2023; Vetralla *et al*, 2023; Garbincius *et al*, 2023) were tested. *Slc25a28*, which encodes Mitoferrin-2, a Ca^{2+}-independent transporter present in the mitochondrial inner membrane, served as control. This analysis showed that none of the examined members of the mitochondrial Ca^{2+} transport system are differentially expressed in *tmbim5*$^{-/-}$ zebrafish (Fig. EV3), suggesting that none of them compensate for the loss of Tmbim5.

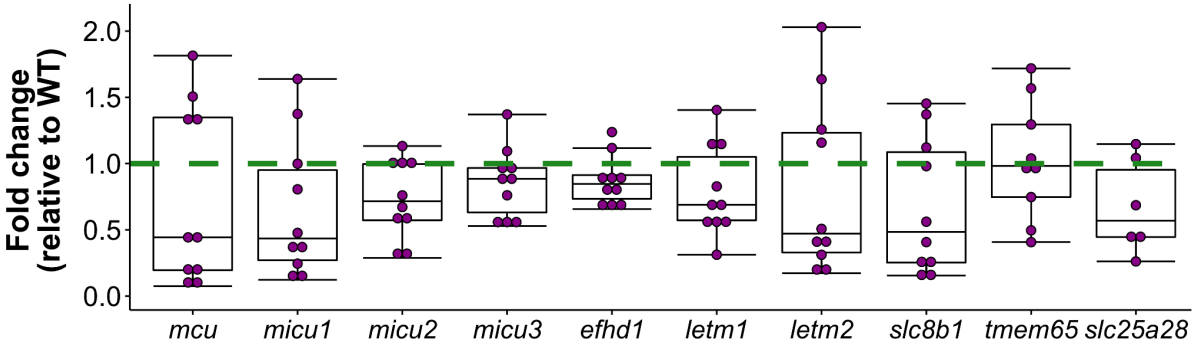

Figure EV3. Tmbim5 deficiency does not affect expression of genes encoding mitochondrial proteins involved in Ca^{2+} transport in zebrafish larvae

mRNA levels of proteins involved in mitochondrial Ca^{2+} transport in 5dpf *tmbim5*$^{-/-}$ larvae quantified with qPCR and normalized to WT, *rpl13a* and *ef1a* were used as reference genes. Results presented as box and whisker plots with the box representing the 25-75th percentile and the whiskers indicating min to max, each dot representing an independent biological replicate, n = 6-10 (each RNA sample was isolated from 30 larvae), number of experiments = 5, one sample *t* test with BH correction for the multiply comparisons.

No severe phenotype of fish lacking the NCLX ortholog Slc8b1 and Tmbim5

Sodium-dependent mitochondrial Ca^{2+} release is mediated by NCLX (Palty *et al*, 2010). To investigate potential functional interactions between Nclx and Tmbim5, we next generated a double knockout zebrafish line lacking both Tmbim5 and the predicted Nclx. Similar to Mcu, we assumed that depletion of two (potentially independent) mitochondrial Ca^{2+} release systems would be detrimental as shown in cell culture where loss of TMBIM5 with concurrent inactivation of NCLX by *NCLX* silencing or treatment with CGP resulted in a reduced mitochondrial Ca^{2+} buffering capacity (Austin *et al*, 2022; Patron *et al*, 2022). The identity of NCLX in fish is unknown but the *slcb81* gene encodes a 308 amino acid protein with the highest homology (24%) to human NCLX and a predicted sodium/calcium exchanger domain at its N-terminus (Fig. EV4A). We designed a gRNA to target this domain which led to the insertion of 17 bp resulting in a frameshift mutation, disrupting the proposed

transporter function of Slc8b1 (Fig. EV4B). It is noteworthy that the predicted fish protein is only half as big as human NCLX which has a length of 584 amino acids.

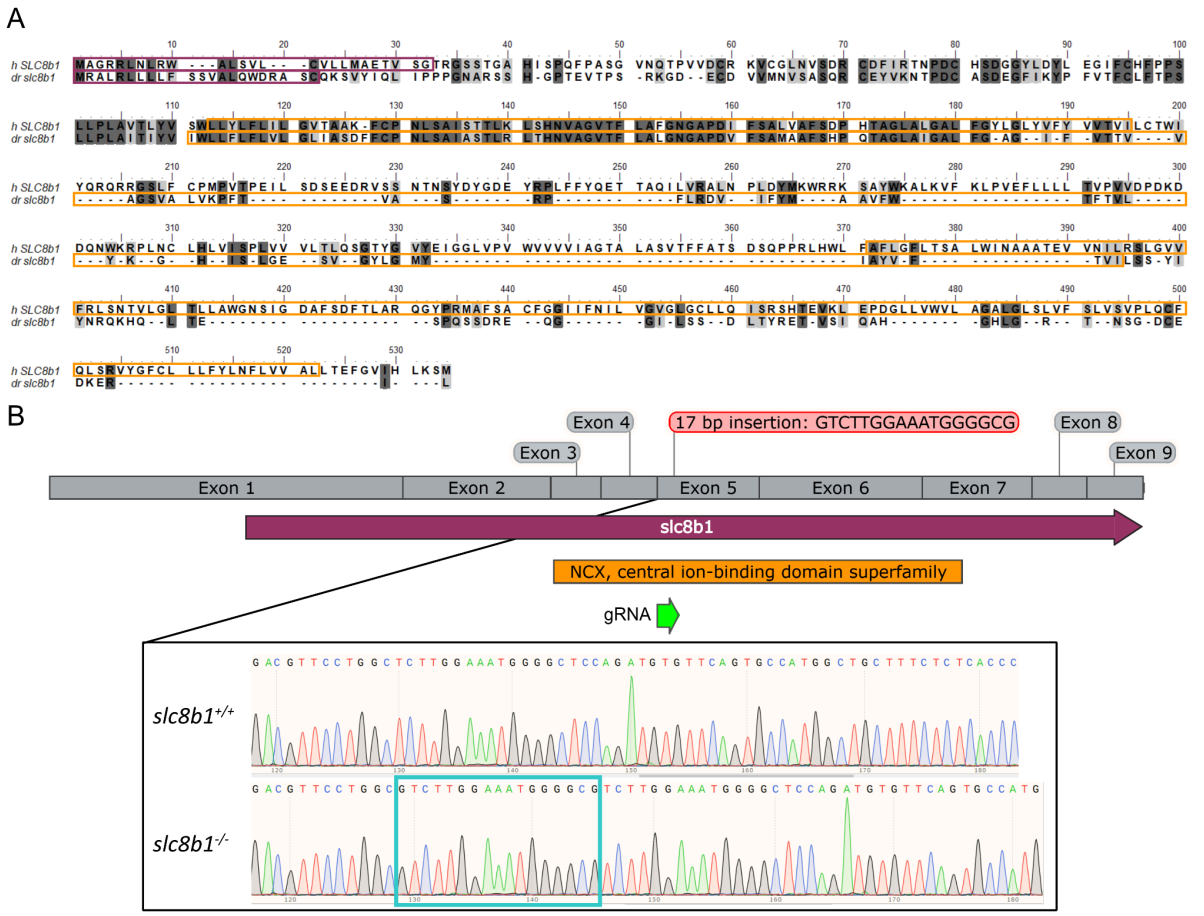

Figure EV4. Generation of Slc8b1-deficient fish

A) Comparison of human and zebrafish NCLX encoded by *slc8b1*. Sequence alignment using Optimal Global Alignment with BLOSUM62 similarity matrix showed 24% of identity between sequences. Identical residues are marked with dark gray and residues with similar physico-chemical properties are marked with light gray. Predicted signal peptide is marked with a violet frame and sodium/calcium domain is marked with an orange frame.

B) Scheme presenting the site of mutation in *slc8b1* with results of Sanger's sequencing (inserted base pairs are marked with a turquoise frame).

s*lc8b1* (*nclx*) mRNA levels peaked at six hours post fertilization and declined thereafter (Fig. 5A). In situ hybridization revealed that *slc8b1* is strongly expressed in the brain and in neuromasts, which are sensory patches distributed on the head and along the lateral line of fish (Metcalfe *et al*, 1985), indicating some overlap with *tmbim5* expression (Fig. 5B). In adult fish, *tmbim5* and *slc8b1* are both expressed in the brain but only *tmbim5* is expressed in skeletal muscles (Fig. 5C).

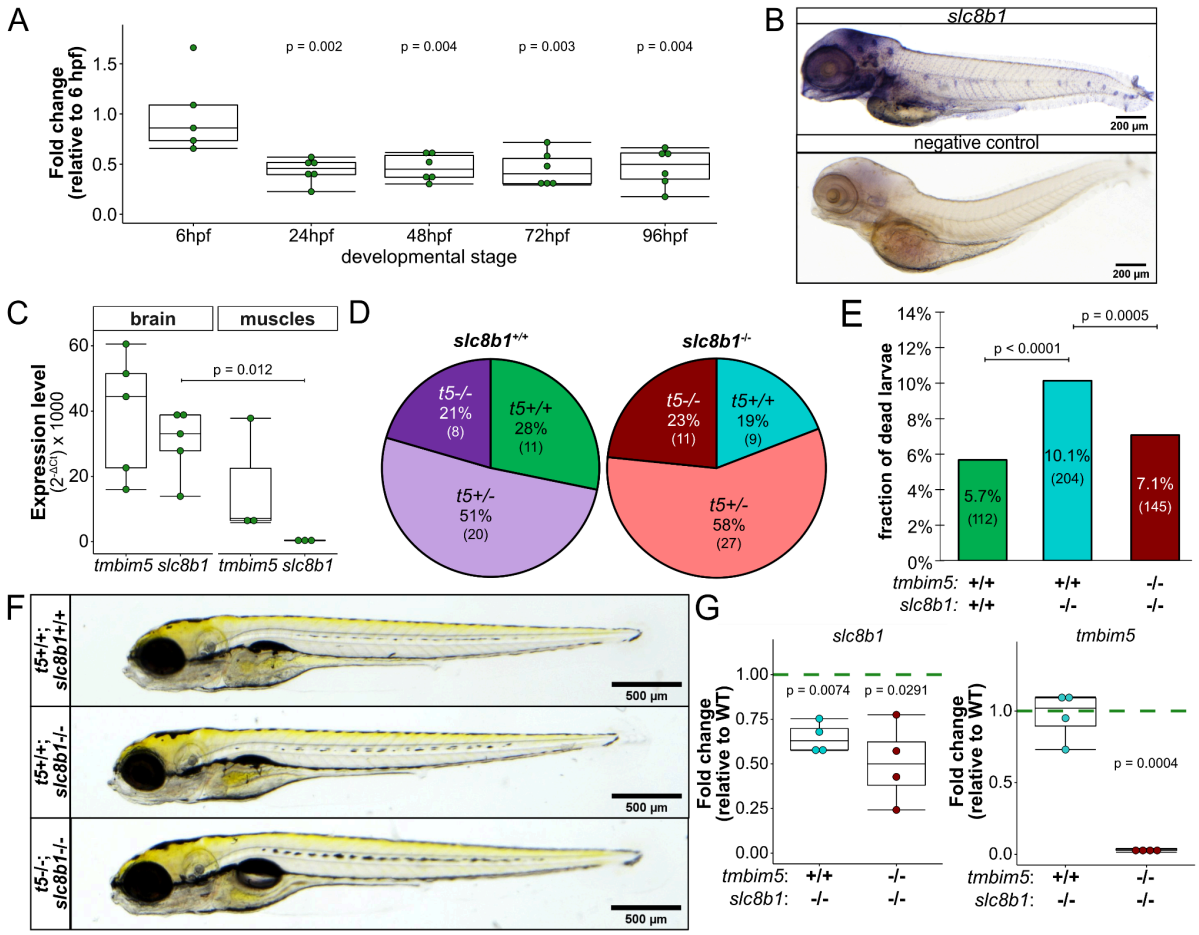

Figure 5. Phenotype of fish lacking the NCLX ortholog Slc8b1 and Tmbim5

A) *slc8b1* mRNA levels at different developmental stages estimated using qPCR, *18S* was used as a reference gene, expression normalized to 6 hpf. Results presented as box and whisker plots with the box representing the 25-75th percentile and the whiskers indicating min to max, each dot representing an independent biological replicate, n = 5-6 (each RNA sample was isolated from 30 embryos), number of experiments = 4, one-way ANOVA followed by post-hoc Tukey HSD test, p values for comparisons with 6 hpf.

B) *slc8b1* transcript detected with whole-mount in situ hybridization in 4 dpf wild-type, sense probe was used as a negative control, number of experiments = 3.

C) Expression pattern of *slc8b1* in the brain and skeletal muscles of adult zebrafish in comparison to *tmbim5*. Results presented as box and whisker plots with the box representing the 25-75th percentile and the whiskers indicating min to max, each dot representing an independent biological replicate, n = 3-5 (each RNA sample was isolated from 2 fish), number of experiments = 2-3, *t* test with BH correction for the multiply comparisons.

D) Genotype distribution does not differ from expected after *tmbim5*$^{+/-}$;*slc8b1*$^{+/-}$ zebrafish breeding.n is indicated in brackets, number of experiments = 3, compared to Mendelian distribution with Chi-square test.

E) Mortality of *slc8b1*$^{-/-}$ larvae until 5 dpf is lower than survival of wild-type or *tmbim5*$^{-/-}$;*slc8b1*$^{-/-}$ double KO larvae, n is indicated in brackets, Chi-square test.

F) Normal morphology of 5 dpf *tmbim5*$^{-/-}$;*slc8b1*$^{-/-}$ double KO larvae. Representative images of WT, *nclx*$^{-/-}$ and *tmbim5*$^{-/-}$;*slc8b1*$^{-/-}$ larvae.

G) *slc8b1* and *tmbim5* mRNA level in 5dpf *tmbim5*$^{+/+}$;*slc8b1*$^{-/-}$ and *tmbim5*$^{-/-}$;*slc8b1*$^{-/-}$ larvae quantified with qPCR and normalized to WT, *rpl13a* and *ef1a* were used as reference genes. Results presented as box and whisker plots with the box representing the 25-75th percentile and the whiskers indicating min to max, each dot representing an independent biological replicate, n = 4 (each RNA sample was isolated from 30 larvae), one sample *t* test with BH correction for the multiply comparisons.

slc8b1 knockout fish were viable and did not exhibit severe phenotypic alterations (Fig. 5D-F). However, it is important to note that the phenotypic characterization of Slc8b1-deficient zebrafish was not as comprehensive as the in-depth analysis performed for Tmbim5-deficient fish as we mainly generated these fish to study crosstalk between Slc8b1

and Tmbim5. *slc8b1* mRNA was reduced but not absent in knockout fish and we observed no compensatory changes of *tmbim5* mRNA in single *slc8b1* and in double-knockout fish (Fig. 5G). The Mendelian distribution of *tmbim5* wildtype and mutants was not affected by concomitant absence of Slc8b1 (Fig. 5D). There was, however, an increased mortality of *slc8b1*$^{-/-}$ (*tmbim5*$^{+/+}$;*slc8b1*$^{-/-}$) fish at the larval stage which was rescued by *tmbim5*$^{-/-}$;*slc8b1*$^{-/-}$ double KO (Fig. 5E). This protective effect is again counterintuitive because if both proteins mediated efflux concomitant knockout should exacerbate the phenotype. This suggests that Tmbim5 and Slc8b1 have opposing functions in mitochondrial Ca^{2+} transport, instead of both mediating efflux.

Abolished behavioral response to CGP in Tmbim5-deficient zebrafish

To further investigate the potential interplay between Tmbim5 and Slc8b1 without risking damage to vulnerable mitochondria during isolation, we used behavioral changes induced by the Nclx inhibitor CGP as a readout in intact zebrafish. We found that CGP added to the bath reduced locomotor activity of wild-type zebrafish measured by velocity and total distance covered within a few hours. This allowed us to compare locomotor activity of wild-type, *tmbim5*- and *slc8b1*-deficient, and double-knockout larvae. We found no significant differences between genotypes in not-treated larvae (Fig. 6A). Surprisingly, WT, *slc8b1*$^{-/-}$ and double *tmbim5*$^{-/-}$;*slc8b1*$^{-/-}$ larvae exhibited a reduction in locomotor activity during a five-hour treatment while *tmbim5*$^{-/-}$ mutant fish were unresponsive (Fig. 6A). These changes are specific to CGP, because WT and *tmbim5*$^{-/-}$ mutant fish both reacted similarly to CCCP with an initial increase in locomotor activity, followed by a gradual reduction in mobility over the course of one hour (Fig 6B). These results suggest that Tmbim5 deficiency confers a partial protection against the effects of CGP *in vivo*. These results are unexpected, as they again contradict the hypothesis that Tmbim5 functions as an additional non-sodium-dependent mitochondrial Ca^{2+} efflux pathway. If this were the case, one would anticipate a more pronounced effect of CGP, which inhibits the remaining Nclx-mediated efflux, in the absence of Tmbim5. It is, however, in line with the reduced mortality of Slc8b1-depleted zebrafish in double *tmbim5*$^{-/-}$;slc8b1$^{-/-}$ KO fish. Together these results suggest that Slc8b1 is not the target of CGP and that neither Tmbim5 nor Slc8b1 constitutes the major mitochondrial Ca^{2+} efflux transport system in zebrafish.

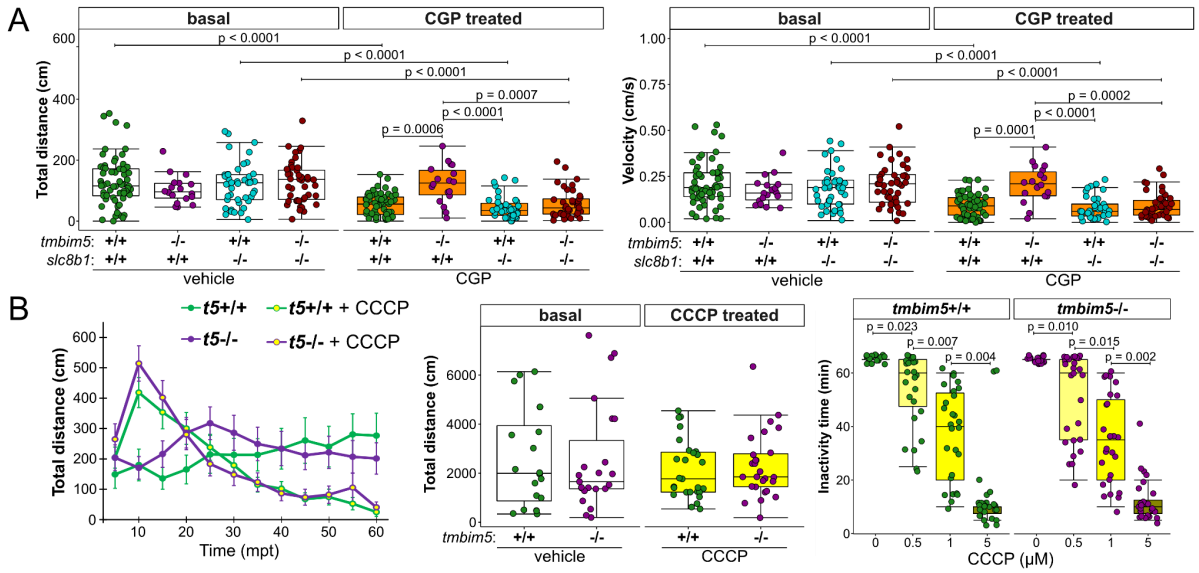

Figure 6. Altered behavioral response to CGP in Tmbim5-deficient zebrafish

A) WT, *slc8b1*$^{-/-}$ and double knockout *slc8b1*$^{-/-}$;*tmbim5*$^{-/-}$ larvae decreased their locomotor activity after 5 hours of treatment with CGP-37157 (5 μM), but this effect was not observed in *tmbim5*$^{-/-}$ zebrafish. On the left, total distance and on the right, mean velocity after 5 hours of treatment were plotted as box and whisker plots with the box representing the 25-75th percentile and the whiskers indicating min to max, each dot representing an individual larvae, n = 18-64, number of experiments = 3, Two-way ANOVA followed by *t* test or Mann–Whitney test (the effect of treatment) and Kruskal-Wallis and Dunn's test (the effect of genotype).

B) Treatment with CCCP (1 μM) had a similar effect on WT and *tmbim5*$^{-/-}$ zebrafish larvae behavior. On the left, total distance covered by each larvae during 5 min of recording while animals were treated with CCCP. Data are presented as mean ± SEM. On the right, total distance covered during 1 hour of treatment did not differ between the groups and inactivity time decreased during CCCP treatment in a dose-dependent manner, but was not affected by loss of Tmbim5. Data was plotted as box and whisker plots with the box representing the 25-75th percentile and the whiskers indicating min to max, each dot representing an individual larvae, n = 20-27, number of experiments = 4, Two-way ANOVA followed by Kruskal-Wallis and Dunn's test.

Discussion

We found that Tmbim5, a less-studied inner mitochondrial membrane ion transporter, is essential for growth, muscle function, metabolism, and mitochondrial membrane potential in zebrafish, but not for steady-state mitochondrial Ca^{2+} levels. Double knockout of Tmbim5 and major mitochondrial Ca^{2+} transport systems caused no severe phenotype, suggesting that Tmbim5 does not compensate for their loss and other Ca^{2+} transport mechanisms exist.

Tmbim5 deficiency decreased the size of zebrafish larvae and weight of adults in line with knockdown of the *tmbim5* ortholog in snails (Yu *et al*, 2020) but not in mice (Zhang *et al*, 2022). However, similar to *Tmbim5* mutant mice that suffer from myopathy, myofiber cross-sections were smaller in *tmbim5*$^{-/-}$ fish, indicating muscle atrophy. Glycogen was reduced in skeletal muscle and liver of *tmbim5*$^{-/-}$ fish and the intermuscular spaces were intensely stained with Alcian blue suggesting the accumulation of glycosaminoglycans. Both abnormalities probably correspond to ATP deficiency which has been reported as a common effect of TMBIM5 loss in cell lines (Seitaj *et al*, 2020; Patron *et al*, 2022; Zhang *et al*, 2022). Accumulation of glycosaminoglycans are also in line with mitochondrial dysfunction, impaired oxidative phosphorylation, and oxidative stress (Stepien *et al*, 2020)(Montero *et al*, 2019; Yubero *et al*, 2016)(Oller *et al*, 2021). These pathological alterations of muscle function probably underlie the delayed escape of Tmbim5-deficient embryos from the chorion which is mediated by tail coiling (Lessman & Carver, 2014). Interestingly, also *Mcu* knockout in mice negatively affects size (Pan *et al*, 2013) and affects proper skeletal muscle trophism (Mammucari *et al*, 2015; Gherardi *et al*, 2019). MICU1-deficient mice also showed severe growth defects (Liu *et al*, 2016) and marked muscle weakness, easy fatigue and smaller muscle fibers (Liu *et al*, 2016; Debattisti *et al*, 2019). In addition, loss-of-function mutations in human *MICU1* are associated with myopathy (Logan *et al*, 2014; Lewis-Smith *et al*, 2016; Bitarafan *et al*, 2021). Together these observations corroborate the role of Tmbim5 in the regulation of growth and muscle function and point out similarities between the effects of Tmbim5, Mcu and Micu1 loss.

Two recent studies demonstrated that TMBIM5 functions as a pH-dependent mitochondrial Ca^{2+} efflux transporter (Patron *et al*, 2022; Austin *et al*, 2022). Zhang et al., in contrast, found that TMBIM5 overexpression in HEK cells enhanced mitochondrial Ca^{2+} uptake following ER Ca^{2+} release (Zhang *et al*, 2022), suggesting that TMBIM5 may operate bidirectionally under certain conditions. To clarify the physiological relevance of this, we now generated two double knockout zebrafish lines: one lacking both Tmbim5 and Mcu, the primary mitochondrial Ca^{2+} influx mediator, and another deficient in Tmbim5 and Slc8b1, the zebrafish ortholog of NCLX, major mitochondrial Ca^{2+} efflux pathway. Surprisingly, both double knockout lines were viable and exhibited no overt phenotypic alterations. Loss of Tmbim5 even protected against an increase in mortality observed in *slc8b1* KO fish making it rather improbable that both proteins mediate mitochondrial Ca^{2+} efflux as lack of both pathways would probably trigger a pathological response. One possible mechanism of protection is the limitation of mitochondrial Ca^{2+} uptake. This protective effect may not

necessarily be a direct consequence of Tmbim5 functioning as a Ca^{2+} transporter, but Tmbim5 could modulate Ca^{2+} influx through its interaction with the MCU complex. Recent evidence suggests that TMBIM5 is a member of the MCU interactome (Delgado de la Herran *et al*, 2024). Furthermore, TMBIM5 has been shown to inhibit the m-AAA protease subunit AFG3L2 (Patron *et al*, 2022), which is responsible for degrading EMRE (König *et al*, 2016; Tsai *et al*, 2017), a crucial component of the MCU complex required for its proper assembly and function. Therefore, the absence of Tmbim5 could lead to an overactivation of the m-AAA protease, resulting in increased EMRE degradation and, consequently, reduced Ca^{2+} influx through the MCU complex.

Our contribution is the first to describe the presence, expression pattern and the loss-of-function phenotype of the probable NCLX ortholog encoded by *slc8b1* in zebrafish. Similar to mouse NCLX (Luongo *et al*, 2017), zebrafish *slc8b1* is mainly expressed in the nervous system. However, its knockout does not cause early embryonic lethality as has been described for the mouse ortholog (Luongo *et al*, 2017). However, also MCU deficiency causes no major phenotype in zebrafish (Soman *et al*, 2019b; Tomar *et al*, 2019; Langenbacher *et al*, 2020) but causes lethality in mice, at least in the C57Bl/6 background [Citation error]. It is noteworthy, that the protein encoded by zebrafish *slc8b1* is considerably smaller than human NCLX, roughly half the size, making it possible that homodimers of zebrafish Slc8b1 could work as NCLX. At this time, we cannot rule out that zebrafish do not have a *bona fide* homolog. Also the similar effects of CGP, which reduced locomotor activity, in both wild-type zebrafish and in zebrafish lacking Slc8b1, suggest that Slc8b1 might not be the primary target of CGP in zebrafish. Alternatively, this could be caused by known pleiotropic effects of this compound, which also inhibits voltage-dependent Ca^{2+} channels (Ruiz *et al*, 2014) and sarco/endoplasmic reticulum Ca^{2+}-ATPase (SERCA) activity (Neumann *et al*, 2011), while activating ryanodine receptor channels (Neumann *et al*, 2011). Astonishingly, the double knockout of *tmbim5*/*slc8b1* reacted to CGP similar to wildtype and was not resistant to CGP like *tmbim5* KO alone. Further investigation is needed to address the transport capacity of Slc8b1 in more detail and to elucidate the specific role of Tmbim5 in mediating the effects of CGP in zebrafish.

We conclude that this lack of a strong phenotype in double knockout fish for influx and efflux pathways suggests the presence of robust compensatory mechanisms or the existence of alternative pathways that can maintain mitochondrial Ca^{2+} homeostasis in the absence of Tmbim5 and Mcu/Slc8b1. So which other proteins could do the job? LETM1 has been postulated to mediate mitochondrial H^+-dependent Ca^{2+} efflux (Jiang *et al*, 2009) and LETM1-containing liposomes were able to accumulate Ca^{2+} (Jiang *et al*, 2009; Tsai *et al*, 2014; Shao *et al*, 2016), but its function as a Ca^{2+} transporter is still in dispute. Austin et al. observed that inhibiting the potassium-hydrogen exchanger with quinine reduced mitochondrial Ca^{2+} efflux. They interpreted this finding as evidence that LETM1 might influence mitochondrial Ca^{2+} efflux by directly regulating monovalent cation levels rather than by directly transporting Ca^{2+} itself (Austin *et al*, 2017). Interestingly, LETM1 might interact with TMBIM5 (Austin *et al*, 2022). Another recently identified candidate for Ca^{2+} efflux is TMEM65 (Garbincius *et al*, 2023; Vetralla *et al*, 2023; Zhang *et al*, 2023). However, TMEM65-mediated Ca^{2+} efflux can also be inhibited by CGP as well as by *NCLX* knockout, indicating that this protein is an essential NCLX regulator and not an independent transporter (Garbincius *et al*, 2023; Vetralla *et al*, 2023).

In conclusion, loss of Tmbim5 impairs zebrafish growth, increases cell death in the brain and results in abnormal mitochondrial function as evidenced by reduced mitochondrial membrane potential and altered metabolism. However, the absence of Tmbim5 did not affect mitochondrial Ca^{2+} levels or exacerbate the phenotype of either *mcu* or *slc8b1* knockout

zebrafish. This study demonstrated that mitochondrial Ca^{2+} homeostasis can still be maintained in the absence of Tmbim5 and Mcu or Slc8b1. Thus, alternative pathway(s) of mitochondrial Ca^{2+} influx and efflux compensate for the loss of these proteins.

Methods

Reagents and Tools table

Reagent/Resource	Reference or Source	Identifier or Catalog Number
Experimental Models: *Danio rerio*		
AB (wild-type)	Zebrafish Core Facility, IIMCB, Poland	ZDB-GENO-960809-7
tmbim5 (*ghitm*)$^{-/-}$	(Gasanov *et al*, 2021) Prof. Jacek Kuźnicki, IIMCB, Poland	-
Tg(HuC:CEPIA2mt)	Prof. Jacek Kuźnicki, IIMCB, Poland	-
mcu$^{-/-}$	(Soman *et al*, 2019a) Prof. Jacek Kuźnicki, IIMCB, Poland	-
slc8b1(nclx)$^{-/-}$	This study	-
Antibodies:		
Alkaline phosphatase-conjugated anti-DIG antibody	Roche	11093274910
Oligonucleotides and other sequence-based reagents:		
Oligonucleotides for gRNA synthesis gRNA for generation of *tmbim5*$^{-/-}$ line	(Gasanov *et al*, 2021)	-
Primers for *tmbim5*$^{-/-}$ genotyping	(Gasanov *et al*, 2021)	-
Oligonucleotide for gRNA synthesis for generation of *slc8b1*$^{-/-}$ line	This study Sigma-Aldrich	TAATACGACTCACTATAGGAGTGACGTTC CTGGCTCTGTTTTAGAGCTAGAA
Constant oligonucleotide for gRNA synthesis	(Gasanov *et al*, 2021)	-
Primers for *slc8b1*$^{-/-}$ genotyping by HRM: FW	This study Sigma-Aldrich	GTGTACCATGTGGATGTGTGTTG
Primers for *slc8b1*$^{-/-}$ genotyping by HRM: RV	This study Sigma-Aldrich	CAGACCAGCAGTTTGAGGGTG
Primers for *slc8b1*$^{-/-}$ genotyping by sequencing: FW	This study Sigma-Aldrich	GAGTTTGCCGTTTAATTTCTGG
Primers for *slc8b1*$^{-/-}$ genotyping by sequencing: RV	This study Sigma-Aldrich	AATTCCTCACCAAAAAGTGCTC
qPCR primers	This study	Table 1

Reagent/Resource	Reference or Source	Identifier or Catalog Number
Primers for riboprobe against *tmbim5* synthesis: FW	This study Sigma-Aldrich	CGCTGCTCAGAGGTGAAGGT
Primers for riboprobe against *tmbim5* synthesis: RV	This study Sigma-Aldrich	TAATACGACTCACTATAGGGATGTGTGCG GCATCTCTGCG
Primers for riboprobe against *slc8b1* synthesis: FW	This study Sigma-Aldrich	GTGTAGACGTGCGTTCTTGC
Primers for riboprobe against *slc8b1* synthesis: RV	This study Sigma-Aldrich	TAATACGACTCACTATAGGGACGAGACG CCACAGTAAA
Chemicals, Enzymes and other reagents		
N-phenylthiourea (PTU)	Alfa Aesar	103-85-5
Cas9	(Gasanov *et al*, 2021) Prof. Jacek Kuźnicki, IIMCB, Poland	-
Precision Melt Supermix	BioRad	1725112
MegaScript T7 Transcription Kit	Invitrogen™	A57622
Phenol red solution	Sigma-Aldrich	P0290
BioMix Red	BioLine	BIO-25006
TRI Reagent	Invitrogen™	AM9738
iScript™ cDNA Synthesis Kit	BioRad	1708891
SsoAdvanced Universal SYBR Green Supermix	BioRad	1725274
Phenylmethylsulfonyl fluoride (PMSF)	Roche	10837091001
Protein Assay Dye	Bio-Rad	5000006
Digoxigenin (DIG)-labeled UTP	Roche	11277073910
Paraformaldehyde	Sigma-Aldrich	P6148
Blocking Reagent	Roche	11096176001
Nitro-blue tetrazolium chloride (NBT)	Roche	11383213001
5-bromo-4-chloro-3-indolyl-phosphate (BCIP)	Roche	11383221001
Acridine Orange (AO)	Sigma-Aldrich	A8097
Tricaine	Sigma	A-5040
Low-melting-point agarose	Sigma-Aldrich	A9414
CGP-37157	Sigma-Aldrich	220005

Reagent/Resource	Reference or Source	Identifier or Catalog Number
Carbonyl cyanide 3-chlorophenylhydrazone (CCCP)	Sigma-Aldrich	C2759
Thapsigargin	Invitrogen™	T7459
Oregon Green™ 488 BAPTA-5N hexapotassium salt	Invitrogen™	O6812
Tetramethylrhodamine, Ethyl Ester, Perchlorate (TMRE)	Invitrogen™	T669
Dimethyl Sulfoxide (DMSO)	Sigma-Aldrich	D8418
Software		
Precision Melt Analysis™ Software	Bio-Rad	
SnapGene software	SnapGene	www.snapgene.com
CHOPCHOP	(Labun *et al*, 2019)	https://chopchop.cbu.uib.no
CRISPRscan	(Moreno-Mateos *et al*, 2015)	https://www.crisprscan.org
CFX Maestro Software	Bio-Rad	
ImageJ	(Schneider *et al*, 2012)	https://imagej.nih.gov/ij/
ZEN Microscopy software	Zeiss	
EthoVision XT software	Noldus	
R version 4.1.2		https://www.r-project.org
Other		
CFX Connect RT-PCR Detection System	BioRad	
Borosilicate glass capillaries	Sutter	B100-75-10
P-1000 Flaming/Brown micropipette puller	Sutter	
FemtoJet microinjector	Eppendorf	
ChemiDoc	BioRad	
Nikon SMZ25 stereomicroscope	Nikon	
Zeiss Lightsheet Z.1 microscope	Zeiss	
96-well half-area black polystyrene microplate	Corning®	CLS3694
Tecan Infinite M1000 Pro	Tecan	
ZebraBox	ViewPoint	
ZebraCube	ViewPoint	

Methods and Protocols:

Animal Maintenance

tmbim5$^{+/+}$, *tmbim5*$^{-/-}$, *tmbim5*$^{+/+}$;Tg(*HuC:CEPIA2mt*), *tmbim5*$^{-/-}$;Tg(*HuC:CEPIA2mt*); *tmbim5*$^{+/+}$;*mcu*$^{-/-}$, *tmbim5*$^{-/-}$;*mcu*$^{-/-}$, *tmbim5*$^{+/+}$;*slc8b1*$^{-/-}$ and *tmbim5*$^{-/-}$;*slc8b1*$^{-/-}$ zebrafish were used in the study. All of the animals were maintained according to previously described methods (Matthews *et al*, 2002) in the Zebrafish Core Facility that is a licensed breeding and research facility (PL14656251, registry of the District Veterinary Inspectorate in Warsaw; 064 and 051, registry of the Ministry of Science and Higher Education) at the International Institute of Molecular and Cell Biology in Warsaw. All of the experiments with larvae and adult fish were performed in accordance with the Polish Laboratory Animal Science Association and Local Ethics Committee for Animal Experimentation in Warsaw (permission no. WAW2/050/2022). Adult zebrafish and larvae were kept in E3 medium (2.48 mM NaCl, 0.09 mM KCl, 0.164 mM $CaCl_2 \cdot 2H_2O$, and 0.428 mM $MgCl_2 \cdot 6H_2O$) at 28.5 °C. Larvae were kept in a Petri dish (~50 larvae/dish) in an incubator under a 14 h/10 h light/dark cycle. The stages of fish development were defined as hours postfertilization (hpf) and days postfertilization (dpf). Zebrafish embryos, that were planned to be used in stainings or *in vivo* imaging experiments, were treated with N-phenylthiourea (PTU, Alfa Aesar CAT# 103-85-5) at final concentration of 0.003% to avoid pigmentation. This study is reported in accordance with ARRIVE guidelines (Kilkenny *et al*, 2010).

Generation and genotyping of mutant and transgenic zebrafish lines

Generation of *tmbim5*$^{-/-}$ zebrafish with CRISPR-Cas9 gene editing was previously described in (Gasanov *et al*, 2021). Briefly, a mix of two gRNA: 5'-GGCTGGTATGTGGGAGTCTA-3' and 5'-CGCGGGCAGTGTGGGCCTGA-3' (0.04 mg/ml of each) and Cas9 protein (0.2 mg/ml) were injected into the cytoplasm of one-cell stage wild-type AB zebrafish embryos.

Fish were grown up after injections up to 4-months-old and were fin-clipped for DNA sampling and high resolution melting (HRM) analysis. Targeted region in the 4th exon of *tmbim5* was amplified using Precision Melt Supermix (BioRad, Cat# 1725112), primers: *tmbim5 HRM forward*: 5'-CGATCTGGCCGCAGTACG-3', *tmbim5 HRM reverse*: 5'-CCAGCCAGGAGTTGCTC-3' and the CFX Connect RT-PCR Detection System (BioRad). Melting curve analysis was performed using Precision Melt Analysis (Bio-Rad) software. The mutation-positive ones were analyzed by DNA sequencing. Fish with the deletion of 29 nucleotides and premature STOP codon was selected as F0 founder. F0 fish was outcrossed with the AB zebrafish line, and their mutation-carrying offspring were in-crossed to generate homozygous mutants. Fish were screened via PCR using the same primers as for HRM analysis, followed by Sanger sequencing.

Genotyping of subsequent generations of *tmbim5*$^{+/+}$, *tmbim5*$^{+/-}$ and *tmbim5*$^{-/-}$ fish was based on the difference in the size of PCR product that was detected by electrophoresis in 2% agarose.

To generate double knockout of *tmbim5* and *mcu*, tmbim5-/- zebrafish were outcrossed with *mcu*$^{-/-}$ zebrafish (obtained as a kind gift from prof. Jacek Kuźnicki laboratory). Obtained heterozygous fish were incrossed and their offspring was genotyped for *tmbim5* as described above and for *mcu* as described in (Soman *et al*, 2019a).

To generate zebrafish knockout of *nclx* the exon 5 of *slc8b1* gene was targeted with gRNA designed with free web tools: CHOPCHOP (Labun *et al*, 2019) and CRISPRscan (Moreno-Mateos *et al*, 2015) according to the protocol described in (Wiweger *et al*, 2021). Sequences that were common in both of the predictions and were scored as low risk for off-targets were chosen. The correctness of the sequence in the targeted area in the AB

zebrafish was confirmed by Sanger sequencing. The gene-specific oligonucleotide with T7 overlaps: 5'-taatacgactcactataGGAGTGACGTTCCTGGCTCTgttttagagctagaa-3'. During gRNA preparation, annealing and filling in steps were combined, and the template was prepared by PCR using BioMix Red (BioLine, Cat# BIO-25006), gene-specific and constant oligo: 5'-AAAAGCACCGACTCGGTGCCACTTTTTCAAGTTGATAACGGACTAGCCTTATTTT AACTTGCTATTTCTAGCTCTAAAAC-3' (10 µM). The PCR conditions were the following: pre-incubation at 95°C for 3 min, followed by 35 cycles of 95°C for 15 s, 40°C for 15 s, and 68°C for 15 s. sgRNA was prepared using 150 ng of purified PCR product and MegaScript T7 Transcription Kit (Invitrogen, Cat# A57622) according to the manufacturer's recommendations. Thereafter, RNA was precipitated by overnight incubation with ammonium acetate at -20°C.

gRNA was suspended in water, and the concentration was adjusted to 500 ng/µl. Cas9 protein (14 mg/ml stock, made in-house) was diluted in KCl/HEPES (200 mM/10 mM, pH 7.5) buffer to a final concentration of 600 ng/µl. The injection mixture was assembled fresh by mixing 2 µl of gRNA (1 µg), 2 µl of Cas9 (1.2 µg), and 0.5 µl phenol red (Sigma, Cat# P0290) and left for complex formation at room temperature for 5–10 min. Thereafter, the samples were kept on ice. Microneedles were pulled from borosilicate glass capillaries (Sutter; Cat# B100-75-10) using a P-1000 Flaming/Brown micropipette puller (Sutter). One nanoliter of the gRNA/Cas9/phenol red mixture was injected into the yolk at 1–2 cell-stage *tmbim5*$^{-/-}$ zebrafish embryos using a FemtoJet microinjector (Eppendorf).

Fish were grown up after injections up to 4-months-old and were fin-clipped for DNA sampling and high resolution melting (HRM) analysis. Targeted region in the 5th exon of *scl8b1* was amplified using Precision Melt Supermix (BioRad, Cat# 1725112), primers: *slc8b1 HRM forward*: 5'-GTGTACCATGTGGATGTGTGTTG-3', *slc8b1 HRM reverse*: 5'-CAGACCAGCAGTTTGAGGGTG-3' and the CFX Connect RT-PCR Detection System (BioRad). Melting curve analysis was performed using Precision Melt Analysis (Bio-Rad) software. The mutation-positive ones were analyzed by DNA sequencing of PCR products. Samples for sequencing were prepared by PCR using BioMix Red (BioLine, Cat# BIO-25006), *slc8b1 seq forward*: 5'-GAGTTTGCCGTTTAATTTCTGG-3', *slc8b1 seq reverse*: 5'-AATTCCTCACCAAAAAGTGCTC-3' and 2 µl of gDNA template per 20 µl of reaction. Fish with the confirmed insertions or deletions leading to premature STOP codon were selected as F0 founders. F0 fish was outcrossed with the AB zebrafish line, and their mutation-carrying offspring were in-crossed to generate double-homozygous mutants. Fish were screened via HRM analysis, followed by Sanger sequencing.

For *in vivo* mitochondrial Ca^{2+} imaging experiments *tmbim5*$^{-/-}$ fish were outcrossed with Tg(*HuC:CEPIA2mt*) zebrafish (obtained as a kind gift from prof. Jacek Kuźnicki laboratory). Their offspring were sorted for CEPIA2mt signal in the brain under the fluoroscope between 2 to 4 dpf.

Quantitative Real-Time PCR

Total RNA was extracted using TRI Reagent (Invitrogen, Cat# AM9738) according to a previously published protocol (Peterson & Freeman, 2009). Thirty embryos or larvae or organs dissected from two adult zebrafish were pooled together to obtain one RNA sample. RNA quality was verified by measuring absorbance at 260, 280, and 230 nm. Only samples with absorbance >1.8 at A260/280 nm were used for further processing. 500 ng of RNA was used for cDNA synthesis with iScript™ cDNA Synthesis Kit (BioRad, Cat# 1708891).

qRT-PCR was performed in duplicate using 25 ng of cDNA, SsoAdvanced Universal SYBR Green Supermix (BioRad, Cat# 1725274) and 0.25 µM of each primer. The primers that were used for qRT-PCR are listed in Table 1. Gene expression levels were analyzed using

the CFX Connect Real-time PCR Detection System (Bio-Rad). Fold changes were calculated using the ΔΔCq method. *Eukaryotic translation elongation factor 1 α1, like 1* (*ef1a*) and *ribosomal protein L13a* (*rpl13a*) or *18S ribosomal RNA* (*18S*) (for *tmbim5* and *slc8b1* expression analysis during the development) were used as housekeeping genes for normalization. Changes in expression are expressed as fold changes using expression in WT as a reference value. The calculations were performed in Microsoft Excel.

Gene name	Abbreviation	Primer sequence	
		Forward	Reverse
transmembrane BAX inhibitor motif-containing protein 5 (growth hormone inducible transmembrane protein)	*tmbim5 (ghitm)*	GTCTCGGCATGTCCAGTGAG	CATGATCCCCATGAGCACCG
mitochondrial calcium uniporter	*mcu*	GTATCCCGCATTCGGTGTCT	CTGTTCTCAGACCGTGTGCT
mitochondrial calcium uptake 1	*micu1*	GACGGAGAGGTTGACCTTGA	GCGATCTCGGTGTCTCATCC
mitochondrial calcium uptake 2	*micu2*	ACCAAAGCAGACTTGGACGAA	GATCAACCCCTTGTCACCGA
mitochondrial calcium uptake family, member 3a	*micu3a*	TGCCGTTCCATTGGACAAGA	TGGTGTTAACCAGGTGTCGG
EF-Hand Domain Family Member D1	*efhd1*	ATCGACGTGTCCACTGAAGG	TCAGCCTCGAACTTACTGCG
leucine zipper-EF-hand containing transmembrane protein 1	*letm1*	GGTGGATGCAGAACACGCT	TCGCTCAGCATGTCAATCTCC
leucine zipper-EF-hand containing transmembrane protein 2	*letm2*	CCGATCTGACACCATACCCG	TCAGGCGTCCTGTCGAAAAA
solute carrier family 8 member B1	*slc8b1*	CGGAGTTCACACGGACCTAC	GATGGCTAGGGGCAGAAGAC
eukaryotic translation elongation factor 1 α1, like 1	*ef1a*	AAAATCGGTGGTGCTGGCAA	GGAACGGTGTGATTGAGGGA
transmembrane Protein 65	*tmem65*	CAACGCCATTCCCTTCATCG	TTCAATCTGAGTGCCAGCGG
solute carrier family 25 member 28 (mitoferrin-2)	*slc25a28*	ACCGGACTATGAGGGTTTGC	AGGCTCTGCATACGTGTCTTT
ribosomal protein L13a	*rpl13a*	TCTGGAGGACTGTAAGAGGTATGC	AGACGCACAATCTTGAGAGCAG
18S ribosomal RNA	*18S*	TCGCTAGTTGGCATCGTTTATG	CGGAGGTTCGAAGACGATCA

Table 1. Primers that were used for qRT-PCR
All primers' sequences are listed as from 5' to 3'.

Whole-mount in situ hybridization (WISH)

Riboprobes for the genes of interest were obtained by PCR using specific primers with T7 overlap at 5' end of reverse: *tmbim5 ISH forward*: 5'-CGCTGCTCAGAGGTGAAGGT-3', *tmbim5 ISH reverse*: 5'-taatacgactcactatagggATGTGTGCGGCATCTCTGCG-3', *slc8b1 ISH*

forward: 5'-GTGTAGACGTGCGTTCTTGC-3', *slc8b1 ISH reverse*: 5'-taatacgactcactatagGG ACGAGACGCCACAGTAAA-3'. Purified PCR products were next utilized in *in vitro* transcription using MegaScript T7 Transcription Kit (Invitrogen, Cat# A57622) and digoxigenin (DIG)-labeled UTP (Roche, Cat# 11277073910) according to the manufacturer's instructions.

Zebrafish larvae were fixed in 4% paraformaldehyde (PFA; Sigma-Aldrich, P6148) in phosphate buffer saline (PBS) overnight at room temperature and stored at -20°C in the methanol. WISH was performed as previously described (Soman *et al*, 2019a) with several modifications. Briefly, after gradual rehydration with PBST (0.1% Tween-20 in PBS), permeabilization with 0.1% sodium citrate and 0.1% Triton X-100 for 10 min on ice, pre-hybridization in Hybridization Solution (HS; 50% deionized formamide, 5X sodium citrate buffer (SSC), 500 µg/ml tRNA, 50 µg/ml heparin, 0.1% Tween-20, 10mM citric acid, 5% sodium dextran sulfate) at 65°C for 3 h, the probes against target mRNAs were added in HS (0.5-3 µg probe/ml buffer) and incubated overnight at 67°C in the water bath. Next, larvae were washed with Hybridization Wash Solution (HWS; 50% deionized formamide, 5X SSC, 0.1% Tween-20, 10mM citric acid) and subsequently with 75% HWS, 50% HWS, 25% HWS in 2X SSCT (SSC with 0.1% Tween-20) and 0.2X SSCT at 65°C. After blocking with 10% Blocking Reagent (Roche, Cat# 11096176001) in Maleic Acid buffer (100mM maleic acid, 100 mM NaCl, 50 mM $MgCl_2$, 0.1% Tween-20) an alkaline phosphatase-conjugated anti-DIG antibody (Roche, Cat# 11093274910) was added to the blocking solution in 1:5000 dilution and incubated overnight at 4°C. Signal was developed by incubation with nitro-blue tetrazolium chloride (0.45 mg/ml, Roche, Cat# 11383213001) and 5-bromo-4-chloro-3-indolyl-phosphate (0.175 mg/ml, Roche, Cat# 11383221001) in Detection buffer (50 mM Tris-HCl pH 9.5, 50 mM NaCl, 25 mM $MgCl_2$, 0.05% Tween 20, 2% polyvinyl alcohol) for 3 h. Background signal was cleaned by 10 min wash with 100% methanol and samples were re-fixed with 4% PFA for 20 min at room temperature and stored in the glycerol until imaging. Imaging was performed using the Nikon SMZ25 stereomicroscope.

Histology

Adult eight-month-old zebrafish were fixed in Bouin's solution, dehydrated in ethanol, xylene and embedded in paraffin. 6 µm thick longitudinal and transverse sections were cut with a Leica microtome (RM2265, Leica) and stained with standard hematoxylin and eosin (H&E). For the determination of glycogen content and mucopolysaccharides accumulation, combined Alcian blue and periodic acid-Schiff (AB/PAS) reactions were performed. The structure of the muscle and connective tissue was visualized using Masson's trichrome stain. Microscopic analysis was carried out using a Nikon Eclipse 90i microscope with a Nikon DS5-U1 camera (Nikon Corporation, Japan) and the computer image analysis system NIS-Elements AR (Nikon Corporation, Japan).

Tetramethylrhodamine ethyl ester (TMRE) microinjections

The stock solution of TMRE (Invitrogen™, Cat# T669) was prepared by dissolving in dimethyl sulfoxide (DMSO, Sigma-Aldrich, Cat# D8418) to a final concentration of 10 mM. Injection solution was prepared at the day of the experiment by diluting 1:5 stock solution in the water (final concentration: 2 mM) and 1 nl was injected into the yolk of embryos at 1-2 cell stage. Microinjections were performed the same as during generation of *nclx*$^{-/-}$ mutants. Embryos were then grown according to standard methods described in the "Animal maintenance" section, but kept in the dark.

In vivo imaging with lightsheet fluorescence microscopy (LSFM)

Stained or transgenic larvae were anesthetized with 0.2 mg/ml Tricaine (Sigma, Cat# A-5040), mounted in 2% low-melting-point agarose (Sigma-Aldrich, Cat# A9414) in a glass capillary and imaged under Zeiss Lightsheet Z.1 microscope using 40X objective (Zeiss) with excitation at 488 nm (AO and *Tg(CEPIA2mt)*) or 561 nm (TMRE). Fish were imaged from the dorsal side of the head and were pushed from capillary to be submerged in the medium from the top of the head up to the middle of the swimming bladder. Measurements were performed at room temperature.

Images were firstly processed in ZEN software (Zeiss) in order to obtain merged maximum projection images, exported to TIF files and analyzed further with ImageJ.

Cell death estimation by Acridine Orange in vivo staining: Acridine Orange (AO; Sigma-Aldrich, Cat# A8097) was added into the plates containing live 4 dpf zebrafish larvae (final concentration: 10 µg/ml E3). After 1 hour of incubation in the dark, the medium was exchanged to fresh E3 six times during 30 min. Z-stacks encompassing 45 µm of optic tectum with 5 µm interval were acquired with Zeiss Lightsheet Z.1 microscope. The counting of the AO-stained cells in the optic tectum of each larvae, that were considered as dying (Pyati *et al*, 2011), was performed manually on the maximum projection images with the CellCounter plug-in in the ImageJ. The number of cells was normalized to the analyzed area of the optic tectum.

Mitochondrial Ca^{2+} flux in the brain of alive zebrafish: In order to estimate mitochondrial Ca^{2+} content 5 dpf larvae, that expressed CEPIA2mt, Ca^{2+} probe targeted to the mitochondria under neural promoter HuC, were treated with 10 µM CCCP (Sigma-Aldrich, Cat# C2759) to induce depolarization of mitochondria and release of mitochondrial Ca^{2+}. Treatment with 5 µM CGP-37157 (Sigma-Aldrich, Cat# 220005) started 5 h before larvae were immobilized. After mounting the zebrafish larvae in the microscopic chamber filled with E3 the medium in the chamber was exchanged to E3 with 10 µM CCCP (Sigma-Aldrich, Cat# C2759). To gain complete depolarization, larvae were treated for 10 min. Z-stacks encompassing 10 µm of optic tectum with 1 µm interval were acquired with Zeiss Lightsheet Z.1 microscope every 5 s during 10 min of treatment.

During image analysis The StackReg plug-in was applied for movement correction. Mitochondria were detected by thresholding and mean fluorescence for mitochondria in the selected square ROI in the optic tectum was calculated. Background fluorescence was calculated as the mean fluorescence of a square that was localized besides the fish, and subtracted from the mean fluorescence of ROI value: $F = F_{ROI} - F_{background}$. F was normalized by the value obtained after full depolarization (F/F_{CCCP}) and the ratio between basal fluorescence (F_0) and F_{CCCP} was calculated to compare mitochondrial Ca^{2+} content between variants similarly to the method described in (Stavsky *et al*, 2021).

Mitochondrial membrane potential (MMP) in vivo measurements: Two days after microinjections with TMRE dechorionated larvae were imaged using LSFM as described above. 2 dpf larvae were treated with 10 µM CCCP (Sigma-Aldrich, Cat# C2759) to induce depolarization of mitochondria. To gain complete depolarization, larvae were treated for 5 min, due to higher toxicity of CCCP treatment at this stage than at 5 dpf. Z-stacks encompassing 10 µm of optic tectum with 1 µm interval were acquired with Zeiss Lightsheet Z.1 microscope every 5 s during 5 min of treatment. F was normalized by the value obtained after full depolarization (F/F_{CCCP}) and the ratio between basal fluorescence (F_0) and F_{CCCP} was calculated to compare mitochondrial membrane potential between variants. Image analysis was performed as for mitochondrial Ca^{2+} measurements described above.

Isolation zebrafish larvae mitochondria

To obtain functional mitochondria from zebrafish 5 dpf larvae a modified method described in (Prudent *et al*, 2013) was used. Larvae (300 - 450 per genotype) were sacrificed by Tricaine treatment and washed with the ice-cold Ringer's buffer (1.8 mM $CaCl_2$, 116 mM NaCl, 2.9 mM KCl, 5 mM HEPES, pH 7.5). Next, rinsed larvae were incubated on ice in the mitochondria isolation buffer (MIB, 210 mM mannitol, 70 mM sucrose, 1mM EDTA, 10mM HEPES, pH 7.5) supplemented with 2 mM PMSF just before usage and transferred to precooled glass-teflon homogenizer in MIB with 2 mM PMSF and BSA (2 mg/ml). Zebrafish tissue was manually homogenized on ice with 50x strokes and centrifuged (1,500 x g, 10 min). Supernatant was transferred to a new tube and centrifuged again to eliminate nuclei and cell debris. After the high-speed centrifugation (14,000 x g, 15 min) of the obtained supernatant, the pellets containing the mitochondria were washed twice with 1 ml ice-cold KCl medium (125 mM KCl, 2 mM K2HPO4, 1 mM $MgCl_2$, 5 mM glutamate, 5 mM malic acid, 20 mM HEPES, pH 7). Pellet was gently resuspended with 0.1 µl of KCl medium per larvae and protein amount was established by Bradford protein assay. During the whole procedure samples were kept on the ice, all centrifugations steps were performed at 4ºC and all used tubes and media were precooled on the ice.

Ca^{2+} measurements in mitochondria isolated from zebrafish larvae

Mitochondrial Ca^{2+} fluxes was measured in freshly isolated mitochondria from 5 dpf zebrafish larvae. 25 µg of mitochondria was gently suspended in KCl medium with glutamate (5 mM), malic acid (5 mM) added freshly and transferred into 96-well half-area black polystyrene microplate (Corning®, Cat# CLS3694). Thapsigargin (0.2 µM, Invitrogen™, Cat# T7459) was added in order to inhibit SERCA pump from potential contaminants from endoplasmic reticulum in the samples. The bath [Ca^{2+}] was detected using the Ca^{2+}-sensitive dye Oregon Green™ 488 BAPTA-5N hexapotassium salt (2 µM, Invitrogen™, Cat# O6812) as described in (Soman *et al*, 2019a). The signal was measured using a plate reader (Tecan Infinite M1000 Pro) at Ex/Em 494/521 nm. Measurements were performed at room temperature.

For the analysis, the first read-out of baseline recording was defined as F_0 and used for normalization. All traces are shown as $\Delta F/F_0$, where $\Delta F = F - F_0$.

Mitochondrial Ca^{2+} uptake assay: 20 µM $CaCl_2$ diluted in KCl medium was added with a multichannel pipette after 30 s of baseline recording. Signal was measured every 3 s for 10 min. Ca^{2+} uptake was calculated as the difference between maximal $\Delta F/F_0$ (first read-out after $CaCl_2$ addition) and $\Delta F/F_0$ value measured 2 min after $CaCl_2$ addition. For the statistical analysis, obtained Ca^{2+} uptake measures were then normalized by the values obtained for WT from the same experiment (samples obtained during one mitochondria isolation process).

Behavioral analysis

Coiling activity of zebrafish embryos: Randomly selected embryos were transferred to a 12-well plate (4 embryos/well) in 2 ml of E3 and acclimated for 2h in 28ºC. Coiling activity was recorded 30 hpf using the Nikon SMZ25 stereomicroscope for 3 min with 10 frames /s acquisition rate. The number of coiling events for each embryo was counted manually.

Open field test: Randomly selected 4 dpf larvae were acclimated to the behavioral testing room for at least 15 min. Two minutes before recording locomotor activity, the larvae were transferred to a 12-well plate that was then placed in the ZebraBox, a high-throughput monitoring system (ViewPoint). The experiment was performed in a volume of 2 mL of E3 medium, and the light intensity was set to 70%. Locomotor activity was recorded for 10 min.

Visual motor response: The experiment was performed according to the procedure described previously (Kedra *et al*, 2020). On the day before the experiment, the larvae were placed in 24-well plates that contained 0.5 mL of E3 medium. Thirty minutes before recording locomotor activity, the plates were placed in the ZebraBox. The experiment consisted of three phases of the following changes in lighting conditions: baseline (0–10 min, 0% light intensity), light (10–20 min, 70% light intensity), and dark (20–30 min, 0% light intensity).

Locomotor response to CGP-37157 treatment: The stock solution of CGP-37157 (Sigma-Aldrich, Cat# 220005) was prepared by dissolving in dimethyl sulfoxide (DMSO, Sigma-Aldrich, Cat# D8418) to a final concentration of 15 mM. On the day of the experiment, the larvae were placed in 24-well plates that contained E3 medium. All wells were filled up to 0.5 ml with a working solution of CGP-37157 or DMSO (both diluted 1:30 in E3, final concentration = 5 μM) and kept in 28°C. 1, 2, 4 and 5 hours after treatment start plates were placed in the ZebraBox for 15 min and locomotor activity of larvae was recorded for 10 min after acclimatization period.

Locomotor response to CCCP treatment: The stock solution of CCCP (Sigma-Aldrich, Cat# C2759) was prepared by dissolving in dimethyl sulfoxide (DMSO, Sigma-Aldrich, Cat# D8418) to a final concentration of 50 mM. On the day of the experiment, the larvae were placed in 24-well plates that contained CCCP diluted in E3 to the final concentration of 0.5 μM, 1 μM and 5 μM. Immediately after beginning of the treatment plates were placed in the ZebraBox for and locomotor activity of larvae was recorded for 60 min.

Novel tank test for adult zebrafish: The 8-months-old zebrafish were acclimated to the behavioral testing room for one week before the experiment. Fish were placed individually in a transparent tank (24 cm length x 14 cm height x 6cm width) filled with aquarium water. ZebraCube, an adult fish monitoring system (ViewPoint) was utilized to record animals' behavior for 15 min.

The video files acquired during experiments with larvae and adult zebrafish were further analyzed using EthoVision XT software (Noldus).

Statistical analysis

All statistical analyses were conducted using R version 4.1.2. Box and whisker plots were generated with R, while other graphs were generated with Microsoft Excel. All datasets were tested for outliers using a Grubbs's test and for normal distribution using the Shapiro-Wilk test. The applied statistical tests are indicated in the figure legends.

Acknowledgments

We thank the Laboratory of Neurodegeneration at IIMCB and specifically Prof. Jacek Kuznicki for providing laboratory space to conduct research on zebrafish, *mcu*$^{-/-}$ and Tg(*CEPIA2mt*) zebrafish lines and helpful discussions. We acknowledge Michał Bazała and Dr Justyna Jędrychowska for generating the Tg(*CEPIA2mt*) zebrafish line. We thank Prof. Jacek Kuźnicki and Prof. Barbara Zabłocka for critical reading of the paper. We acknowledge the IIMCB Zebrafish Core Facility for service and fish material and Microscopy and Cytometry Facility for providing access to LSFM. This research was funded by the National Science Centre, Poland (021/40/C/NZ4/00031) to I.W.

Author contributions

I.W. designed and performed most of the experiments with contributions from S.B. and Ł.M., D.A-U. performed histological analysis of adult zebrafish, A.M. supervised experiments, I.W analyzed data and interpreted results, I.W. and A.M. wrote the manuscript.

Disclosure and competing interests statement

The authors declare no competing interest.

Data availability

This study includes no data deposited in external repositories. No unbiased larger data sets were generated in this study. All data are presented in the results or as supplemental data.

References

Altschuld RA, Hohl CM, Castillo LC, Garleb AA, Starling RC & Brierley GP (1992) Cyclosporin inhibits mitochondrial calcium efflux in isolated adult rat ventricular cardiomyocytes. *Am J Physiol* 262: H1699–704

Austin S, Mekis R, Mohammed SEM, Scalise M, Wang W-A, Galluccio M, Pfeiffer C, Borovec T, Parapatics K, Vitko D, *et al* (2022) TMBIM5 is the Ca /H antiporter of mammalian mitochondria. *EMBO Rep* 23: e54978

Austin S, Tavakoli M, Pfeiffer C, Seifert J, Mattarei A, De Stefani D, Zoratti M & Nowikovsky K (2017) LETM1-Mediated K and Na Homeostasis Regulates Mitochondrial Ca Efflux. *Front Physiol* 8: 839

Baughman JM, Perocchi F, Girgis HS, Plovanich M, Belcher-Timme CA, Sancak Y, Bao XR, Strittmatter L, Goldberger O, Bogorad RL, *et al* (2011) Integrative genomics identifies MCU as an essential component of the mitochondrial calcium uniporter. *Nature* 476: 341–345

Bernardi P, Gerle C, Halestrap AP, Jonas EA, Karch J, Mnatsakanyan N, Pavlov E, Sheu S-S & Soukas AA (2023) Identity, structure, and function of the mitochondrial permeability transition pore: controversies, consensus, recent advances, and future directions. *Cell Death Differ* 30: 1869–1885

Bisbach CM, Hutto RA, Poria D, Cleghorn WM, Abbas F, Vinberg F, Kefalov VJ, Hurley JB & Brockerhoff SE (2020) Mitochondrial Calcium Uniporter (MCU) deficiency reveals an alternate path for Ca uptake in photoreceptor mitochondria. *Sci Rep* 10: 16041

Bitarafan F, Khodaeian M, Amjadi Sardehaei E, Darvishi FZ, Almadani N, Nilipour Y & Garshasbi M (2021) Identification of a novel MICU1 nonsense variant causes myopathy with extrapyramidal signs in an Iranian consanguineous family. *Mol Cell Pediatr* 8: 6

Bultynck G, Kiviluoto S & Methner A (2014) Bax inhibitor-1 is likely a pH-sensitive calcium leak channel, not a H+/Ca2+ exchanger. *Sci Signal* 7: e22

Debattisti V, Horn A, Singh R, Seifert EL, Hogarth MW, Mazala DA, Huang KT, Horvath R, Jaiswal JK & Hajnóczky G (2019) Dysregulation of Mitochondrial Ca Uptake and Sarcolemma Repair Underlie Muscle Weakness and Wasting in Patients and Mice Lacking MICU1. *Cell Rep* 29: 1274–1286.e6

Delgado de la Herran H, Vecellio Reane D, Cheng Y, Katona M, Hosp F, Greotti E, Wettmarshausen J, Patron M, Mohr H, Prudente de Mello N, *et al* (2024) Systematic mapping of mitochondrial calcium uniporter channel (MCUC)-mediated calcium signaling networks. *EMBO J* 43: 5288–5326

De Stefani D, Raffaello A, Teardo E, Szabò I & Rizzuto R (2011) A forty-kilodalton protein of the inner membrane is the mitochondrial calcium uniporter. *Nature* 476: 336–340

Garbincius JF, Salik O, Cohen HM, Choya-Foces C, Mangold AS, Makhoul AD, Schmidt AE, Khalil DY, Doolittle JJ, Wilkinson AS, *et al* (2023) TMEM65 regulates NCLX-dependent mitochondrial calcium efflux. *bioRxiv*

Gasanov EV, Jędrychowska J, Pastor M, Wiweger M, Methner A & Korzh VP (2021) An improved method for precise genome editing in zebrafish using CRISPR-Cas9 technique. *Mol Biol Rep* 48: 1951–1957

Gherardi G, Nogara L, Ciciliot S, Fadini GP, Blaauw B, Braghetta P, Bonaldo P, De Stefani D, Rizzuto R & Mammucari C (2019) Loss of mitochondrial calcium uniporter rewires skeletal muscle metabolism and substrate preference. *Cell Death Differ* 26: 362–381

Jiang D, Zhao L & Clapham DE (2009) Genome-wide RNAi screen identifies Letm1 as a mitochondrial Ca2+/H+ antiporter. *Science* 326: 144–147

Kedra M, Banasiak K, Kisielewska K, Wolinska-Niziol L, Jaworski J & Zmorzynska J (2020) TrkB hyperactivity contributes to brain dysconnectivity, epileptogenesis, and anxiety in zebrafish model of Tuberous Sclerosis Complex. *Proc Natl Acad Sci U S A* 117: 2170–2179

Kettunen P (2020) Calcium Imaging in the Zebrafish. *Adv Exp Med Biol* 1131: 901–942

Kilkenny C, Browne WJ, Cuthill IC, Emerson M & Altman DG (2010) Improving bioscience research reporting: the ARRIVE guidelines for reporting animal research. *PLoS Biol* 8: e1000412

König T, Tröder SE, Bakka K, Korwitz A, Richter-Dennerlein R, Lampe PA, Patron M, Mühlmeister M, Guerrero-Castillo S, Brandt U, *et al* (2016) The m-AAA Protease Associated with Neurodegeneration Limits MCU Activity in Mitochondria. *Mol Cell* 64: 148–162

Labun K, Montague TG, Krause M, Torres Cleuren YN, Tjeldnes H & Valen E (2019) CHOPCHOP v3: expanding the CRISPR web toolbox beyond genome editing. *Nucleic Acids Res* 47: W171–W174

Langenbacher AD, Shimizu H, Hsu W, Zhao Y, Borges A, Koehler C & Chen J-N (2020) Mitochondrial Calcium Uniporter Deficiency in Zebrafish Causes Cardiomyopathy With Arrhythmia. *Front Physiol* 11: 617492

Lessman CA & Carver EA (2014) Zebrafish: Topics in Reproduction, Toxicology and Development Nova Science Publishers

Lewis-Smith D, Kamer KJ, Griffin H, Childs A-M, Pysden K, Titov D, Duff J, Pyle A, Taylor RW, Yu-Wai-Man P, *et al* (2016) Homozygous deletion in MICU1 presenting with fatigue and lethargy in childhood. *Neurol Genet* 2: e59

Liu JC, Liu J, Holmström KM, Menazza S, Parks RJ, Fergusson MM, Yu Z-X, Springer DA, Halsey C, Liu C, *et al* (2016) MICU1 Serves as a Molecular Gatekeeper to Prevent In Vivo Mitochondrial Calcium Overload. *Cell Rep* 16: 1561–1573

Logan CV, Szabadkai G, Sharpe JA, Parry DA, Torelli S, Childs A-M, Kriek M, Phadke R, Johnson CA, Roberts NY, *et al* (2014) Loss-of-function mutations in MICU1 cause a brain and muscle disorder linked to primary alterations in mitochondrial calcium signaling. *Nat Genet* 46: 188–193

Luongo TS, Lambert JP, Gross P, Nwokedi M, Lombardi AA, Shanmughapriya S, Carpenter AC, Kolmetzky D, Gao E, van Berlo JH, *et al* (2017) The mitochondrial Na/Ca exchanger is essential for Ca homeostasis and viability. *Nature* 545: 93–97

Mallilankaraman K, Cárdenas C, Doonan PJ, Chandramoorthy HC, Irrinki KM, Golenár T, Csordás G, Madireddi P, Yang J, Müller M, *et al* (2012a) MCUR1 is an essential component of mitochondrial Ca2+ uptake that regulates cellular metabolism. *Nat Cell Biol* 14: 1336–1343

Mallilankaraman K, Doonan P, Cárdenas C, Chandramoorthy HC, Müller M, Miller R, Hoffman NE, Gandhirajan RK, Molgó J, Birnbaum MJ, *et al* (2012b) MICU1 is an essential gatekeeper for MCU-mediated mitochondrial Ca(2+) uptake that regulates cell survival. *Cell* 151: 630–644

Mammucari C, Gherardi G, Zamparo I, Raffaello A, Boncompagni S, Chemello F, Cagnin S, Braga A, Zanin S, Pallafacchina G, *et al* (2015) The mitochondrial calcium uniporter controls skeletal muscle trophism in vivo. *Cell Rep* 10: 1269–1279

Mandal A, Pinter K & Drerup CM (2018) Analyzing Neuronal Mitochondria in vivo Using Fluorescent Reporters in Zebrafish. *Front Cell Dev Biol* 6: 414920

Matthews M, Trevarrow B & Matthews J (2002) A virtual tour of the Guide for zebrafish users. *Lab Anim* 31: 34–40

Meng K, Hu Y, Wang D, Li Y, Shi F, Lu J, Wang Y, Cao Y, Zhang CZ & He Q-Y (2023) EFHD1, a novel mitochondrial regulator of tumor metastasis in clear cell renal cell carcinoma. *Cancer Sci* 114: 2029–2040

Metcalfe WK, Kimmel CB & Schabtach E (1985) Anatomy of the posterior lateral line system in young larvae of the zebrafish. *J Comp Neurol* 233: 377–389

Montero R, Yubero D, Salgado MC, González MJ, Campistol J, O'Callaghan MDM, Pineda M, Delgadillo V, Maynou J, Fernandez G, *et al* (2019) Plasma coenzyme Q status is impaired in selected genetic conditions. *Sci Rep* 9: 793

Moreno-Mateos MA, Vejnar CE, Beaudoin J-D, Fernandez JP, Mis EK, Khokha MK & Giraldez AJ (2015) CRISPRscan: designing highly efficient sgRNAs for CRISPR-Cas9 targeting in vivo. *Nat Methods* 12: 982–988

Murphy E, Pan X, Nguyen T, Liu J, Holmström KM & Finkel T (2014) Unresolved questions from the analysis of mice lacking MCU expression. *Biochem Biophys Res Commun* 449: 384–385

Neumann JT, Diaz-Sylvester PL, Fleischer S & Copello JA (2011) CGP-37157 inhibits the sarcoplasmic reticulum Ca^2+ ATPase and activates ryanodine receptor channels in striated muscle. *Mol Pharmacol* 79: 141–147

Nowikovsky K, Froschauer EM, Zsurka G, Samaj J, Reipert S, Kolisek M, Wiesenberger G & Schweyen RJ (2004) The LETM1/YOL027 gene family encodes a factor of the mitochondrial K+ homeostasis with a potential role in the Wolf-Hirschhorn syndrome. *J Biol Chem* 279: 30307–30315

Oka T, Sayano T, Tamai S, Yokota S, Kato H, Fujii G & Mihara K (2008) Identification of a novel protein MICS1 that is involved in maintenance of mitochondrial morphology and apoptotic release of cytochrome c. *Mol Biol Cell* 19: 2597–2608

Oller J, Gabandé-Rodríguez E, Ruiz-Rodríguez MJ, Desdín-Micó G, Aranda JF, Rodrigues-Diez R, Ballesteros-Martínez C, Blanco EM, Roldan-Montero R, Acuña P, *et al* (2021) Extracellular Tuning of Mitochondrial Respiration Leads to Aortic Aneurysm. *Circulation* 143: 2091–2109

Orrenius S, Gogvadze V & Zhivotovsky B (2015) Calcium and mitochondria in the regulation of cell death. *Biochem Biophys Res Commun* 460: 72–81

Palty R, Silverman WF, Hershfinkel M, Caporale T, Sensi SL, Parnis J, Nolte C, Fishman D, Shoshan-Barmatz V, Herrmann S, *et al* (2010) NCLX is an essential component of mitochondrial Na+/Ca2+ exchange. *Proc Natl Acad Sci U S A* 107: 436–441

Pan X, Liu J, Nguyen T, Liu C, Sun J, Teng Y, Fergusson MM, Rovira II, Allen M, Springer DA, *et al* (2013) The physiological role of mitochondrial calcium revealed by mice lacking the mitochondrial calcium uniporter. *Nat Cell Biol* 15: 1464–1472

Patron M, Checchetto V, Raffaello A, Teardo E, Vecellio Reane D, Mantoan M, Granatiero V, Szabò I, De Stefani D & Rizzuto R (2014) MICU1 and MICU2 finely tune the mitochondrial Ca2+ uniporter by exerting opposite effects on MCU activity. *Mol Cell* 53: 726–737

Patron M, Tarasenko D, Nolte H, Kroczek L, Ghosh M, Ohba Y, Lasarzewski Y, Ahmadi ZA, Cabrera-Orefice A, Eyiama A, *et al* (2022) Regulation of mitochondrial proteostasis by the proton gradient. *EMBO J*

Peterson SM & Freeman JL (2009) RNA isolation from embryonic zebrafish and cDNA synthesis for gene expression analysis. *J Vis Exp*

Prudent J, Popgeorgiev N, Bonneau B, Thibaut J, Gadet R, Lopez J, Gonzalo P, Rimokh R, Manon S, Houart C, *et al* (2013) Bcl-wav and the mitochondrial calcium uniporter drive gastrula morphogenesis in zebrafish. *Nat Commun* 4: 2330

Pyati UJ, Gjini E, Carbonneau S, Lee J-S, Guo F, Jette CA, Kelsell DP & Look AT (2011) p63 mediates an apoptotic response to pharmacological and disease-related ER stress in the developing epidermis. *Dev Cell* 21: 492–505

Ruiz A, Alberdi E & Matute C (2014) CGP37157, an inhibitor of the mitochondrial Na+/Ca2+ exchanger, protects neurons from excitotoxicity by blocking voltage-gated Ca2+ channels. *Cell Death Dis* 5: e1156

Schneider CA, Rasband WS & Eliceiri KW (2012) NIH Image to ImageJ: 25 years of image analysis. *Nat Methods* 9: 671–675

Seitaj B, Maull F, Zhang L, Wüllner V, Wolf C, Schippers P, La Rovere R, Distler U, Tenzer S, Parys JB, *et al* (2020) Transmembrane BAX Inhibitor-1 Motif Containing Protein 5 (TMBIM5) Sustains Mitochondrial Structure, Shape, and Function by Impacting the Mitochondrial Protein Synthesis Machinery. *Cells* 9

Shao J, Fu Z, Ji Y, Guan X, Guo S, Ding Z, Yang X, Cong Y & Shen Y (2016) Leucine zipper-EF-hand containing transmembrane protein 1 (LETM1) forms a Ca/H antiporter. *Sci Rep* 6: 34174

Soman SK, Bazała M, Keatinge M, Bandmann O & Kuznicki J (2019a) Restriction of mitochondrial calcium overload by inactivation renders a neuroprotective effect in zebrafish models of Parkinson's disease. *Biol Open* 8

Soman SK, Bazała M, Keatinge M, Bandmann O & Kuznicki J (2019b) Restriction of mitochondrial calcium overload by inactivation renders a neuroprotective effect in zebrafish models of Parkinson's disease. *Biol Open* 8

Soman S, Keatinge M, Moein M, Da Costa M, Mortiboys H, Skupin A, Sugunan S, Bazala M, Kuznicki J & Bandmann O (2017) Inhibition of the mitochondrial calcium uniporter rescues dopaminergic neurons in pink1 zebrafish. *Eur J Neurosci* 45: 528–535

Stavsky A, Stoler O, Kostic M, Katoshevsky T, Assali EA, Savic I, Amitai Y, Prokisch H, Leiz S, Daumer-Haas C, *et al* (2021) Author Correction: Aberrant activity of mitochondrial NCLX is linked to impaired synaptic transmission and is associated with mental retardation. *Commun Biol* 4: 755

Stepien KM, Roncaroli F, Turton N, Hendriksz CJ, Roberts M, Heaton RA & Hargreaves I (2020) Mechanisms of Mitochondrial Dysfunction in Lysosomal Storage Disorders: A Review. *J Clin Med Res* 9

Suzuki J, Kanemaru K, Ishii K, Ohkura M, Okubo Y & Iino M (2014) Imaging intraorganellar Ca2+ at subcellular resolution using CEPIA. *Nat Commun* 5: 4153

Tomar D, Jaña F, Dong Z, Quinn WJ 3rd, Jadiya P, Breves SL, Daw CC, Srikantan S, Shanmughapriya S, Nemani N, *et al* (2019) Blockade of MCU-Mediated Ca Uptake Perturbs Lipid Metabolism via PP4-Dependent AMPK Dephosphorylation. *Cell Rep* 26: 3709–3725.e7

Tsai C-W, Wu Y, Pao P-C, Phillips CB, Williams C, Miller C, Ranaghan M & Tsai M-F (2017) Proteolytic control of the mitochondrial calcium uniporter complex. *Proc Natl Acad Sci U S A* 114: 4388–4393

Tsai M-F, Jiang D, Zhao L, Clapham D & Miller C (2014) Functional reconstitution of the mitochondrial Ca2+/H+ antiporter Letm1. *J Gen Physiol* 143: 67–73

Tuckett F & Morriss-Kay G (1988) Alcian blue staining of glycosaminoglycans in embryonic material: effect of different fixatives. *Histochem J* 20: 174–182

Vais H, Mallilankaraman K, Mak D-OD, Hoff H, Payne R, Tanis JE & Foskett JK (2016) EMRE Is a Matrix Ca(2+) Sensor that Governs Gatekeeping of the Mitochondrial Ca(2+) Uniporter. *Cell Rep* 14: 403–410

Vais H, Tanis JE, Müller M, Payne R, Mallilankaraman K & Foskett JK (2015) MCUR1, CCDC90A, Is a Regulator of the Mitochondrial Calcium Uniporter. *Cell Metab* 22: 533–535

Van De Vlekkert D, Machado E & d'Azzo A (2020) Analysis of Generalized Fibrosis in Mouse Tissue Sections with Masson's Trichrome Staining. *Bio Protoc* 10: e3629

Vetralla M, Wischhof L, Cadenelli V, Scifo E, Ehninger D, Rizzuto R, Bano D & De Stefani D (2023) TMEM65-dependent Ca2+ extrusion safeguards mitochondrial homeostasis. *bioRxiv*: 2023.10.10.561661

Vicente M, Salgado-Almario J, Soriano J, Burgos M, Domingo B & Llopis J (2019) Visualization of Mitochondrial Ca Signals in Skeletal Muscle of Zebrafish Embryos with Bioluminescent Indicators. *Int J Mol Sci* 20

Wiweger M, Majewski L, Adamek-Urbanska D, Wasilewska I & Kuznicki J (2021) -Deficient

Zebrafish Reproduce Neurological and Inflammatory Symptoms of Niemann-Pick Type C Disease. *Front Cell Neurosci* 15: 647860

Yubero D, Montero R, O'Callaghan M, Pineda M, Meavilla S, Delgadillo V, Sierra C, Altimira L, Navas P, Pope S, *et al* (2016) Coenzyme Q and Pyridoxal Phosphate Deficiency Is a Common Feature in Mucopolysaccharidosis Type III. *JIMD Rep* 25: 1–7

Yu W, Zhang B, Song H, Zhan R, Li L, He C, Jiang Q, Wang X, Wei L, Zhao N, *et al* (2020) Preliminary investigation demonstrating the GHITM gene probably involved in apoptosis and growth of the golden apple snail (Pomacea canaliculata). *BMC Genomics* 21: 19

Zhang L, Dietsche F, Seitaj B, Rojas-Charry L, Latchman N, Tomar D, Wüst RC, Nickel A, Frauenknecht KB, Schoser B, *et al* (2022) TMBIM5 loss of function alters mitochondrial matrix ion homeostasis and causes a skeletal myopathy. *Life Sci Alliance* 5

Zhang Y, Reyes L, Sun J, Liu C, Springer D, Noguchi A, Aponte AM, Munasinghe J, Covian R, Murphy E, *et al* (2023) Loss of TMEM65 causes mitochondrial disease mediated by mitochondrial calcium. *bioRxiv*: 2022.08.02.502535